VON KARMAN INSTITUTE FOR FLUID DYNAMICS

LECTURE SERIES 1988-04

INTAKE AERODYNAMICS

FEBRUARY 22 - 26, 1988

CFD APPLICATION TO SUBSONIC INLET AIRFRAME INTEGRATION

Bernhard H. Anderson
NASA-Lewis Research Center, Ohio, USA

CFD APPLICATION TO SUBSONIC INLET AIRFRAME INTEGRATION

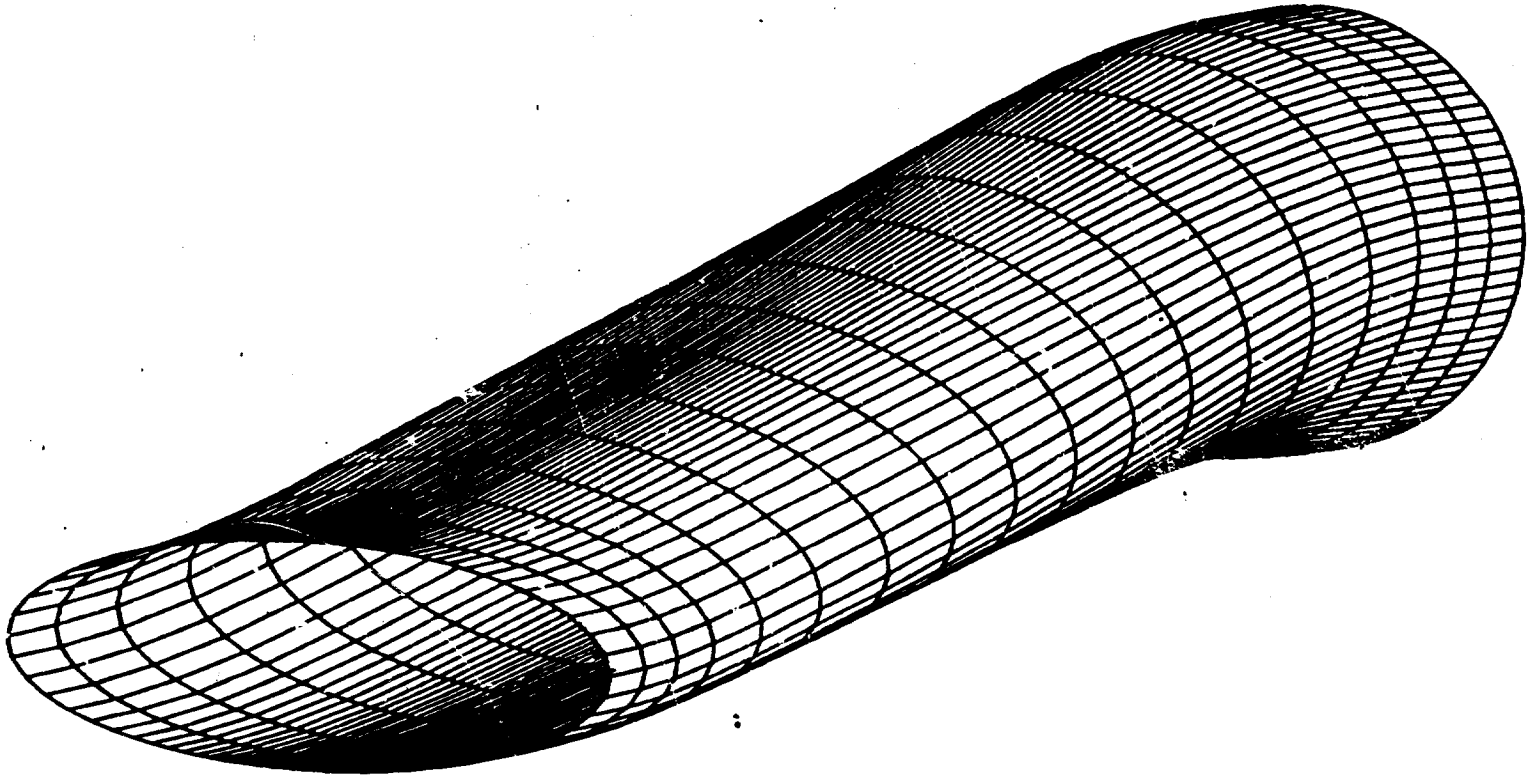

Bernhard H. Anderson
Chief, Computational Methods Branch
NASA Lewis Research Center – Cleveland Ohio – USA

CURRENT REGIME

The class of inlet-airframe sytems that are of most interest today are represented by this figure, where civil applications are shown on the vertical and military type inlet ducts are shown on the horizontal. Civil type inlet-nacelle systems as could be represented by the Boeing 747 are analyzed today using Panal Methods (potential flow analyses), Euler Methods (inviscid), and in some cases, full Navier Stokes methods. These CFD analyses techniques have been discussed in the previous lecture entitled "Computational Methods for Inlet Airframe Integration", by Charles E. Towne, senior research engineer at the NASA Lewis Research Center. This lecture, entitled "CFD Application to Subsonic Inlet-Airframe Integration" will not discuss this type of inlet systems, but will focus on the military class of inlet ducts, which in general, tend to have high L/D design compared to civil systems. The interest today of these systems is towards high tolerance to extreme attitudes and body rates. In these systems, pressure driven secondary flows plays an important role, which is further complicated by high distortion at the inlet face along with the possibility of votex ingestion and internal flow separation, which may be unsteady. This lecture will focus on the basic fluid dynamics of such curved diffuser duct flows using primarily PNS and FNS Navier Stokes techniques CFD techniques.

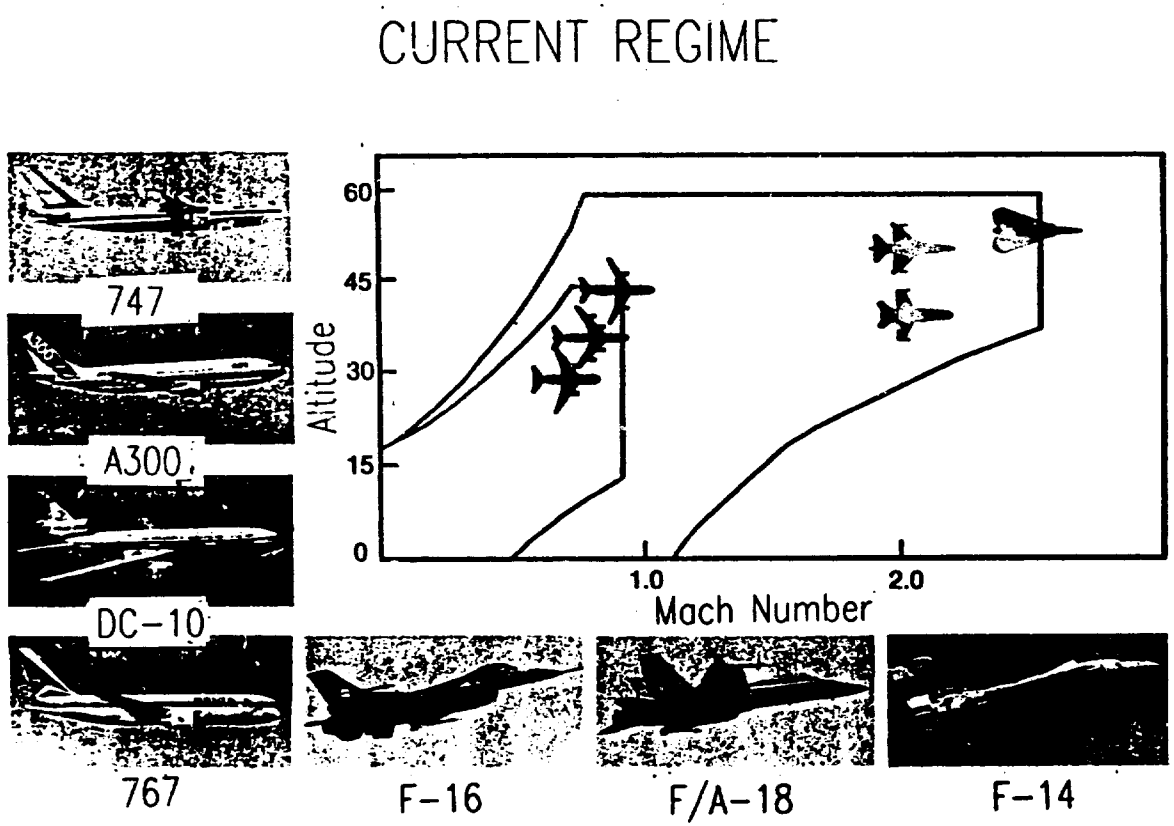

CFD FOR INLET AIRFRAME INTEGRATION

Developing Insight and Understanding

Computational Fluid Dynamics (CFD) is becoming an increasingly powerful tool in the aerodynamic design of aerospace systems, owing to improvements in numerical algorithms, geometric modeling, grid generation, and physical parameter modeling, as well as dramatic improvements in supercomputer processing speed and memory. With the realization of the potential of forthcoming supercomputers, much of the current CFD work will expand to address more complex configurations, geometries, flight regimes, and applications, while some of the existing work will become components of more complex systems of solutions to problems of modeling, grid generation, flow field solution, and flow visualization. Computational Fluid Dynamics is also being used extensively throughout the propulsion community because of a lack of alternatives for achieving insight into the basic controlling mechanisms of the complicated, highly coupled interacting aspects of propulsion fluid dynamics. Thus CFD will become an important aerospace design and development tool requiring a high level of confidence.

To meet the required confidence level, the existing and forthcoming CFD application codes must be verified and validated with the best available experimental data. Because of the complexity of the aerodynamic flows that will be routinely computed, the experimental data base must expand to include not only surface-measurable quantities, but also detailed measurements of fluid and thermal parameters throughout the flow regime of interest. These focused experimental test clearly require detailed flow quantity measurements in addition to integral checks. Also, the errors inherent in experimental testing must be identified, understood, and minimized in order to produce the high-quality, accurate benchmark data that are required for validation of complex CFD applications codes and for use in developing physical modeling data for complex flows.

The concept of "benchmark" or "validation" experiments that highlight one or more basic flow mechanisms important to the inlet airframe system also affords the design engineer the opportunity to study and understand highly complex three dimensional viscous flows from a building block concept, i.e., highly complex viscous flows are composed of "fundamental" or "benchmark" phenomena which interact with each other. With close interaction between CFD and experimentation, advanced computer programs will be used both to design an experiment and to predict the results so that the the test, or design, is under control at all times. But this interaction also gives the researcher a fundamental understanding of the fluid processes that are important to the inlet airframe system under design. This idea is the main thrust of this seminar series on a User's Technology Guide to CFD Inlet Airframe Integration.

CFD FOR INLET AIRFRAME INTEGRATION
Developing Insight and Understanding

"The complementary interplay of CFD and experiment is especially important in the modern world of tailored designs, where the goal is not to generate half-blind global correlations, but to prove the accuracy of a total design system by means of benchmark demonstrations in reliable facilities"

Current Capabilities and Future Direction
in
Computational Fluid Dynamics

CATEGORIES OF CFD-RELATED EXPERIMENTS

Four categories of experimentation were recognized by the Ad Hoc Committee on CFD Validation, NASA Aeronautics Advisory Committee, to be intimately associated with the development of CFD capability, namely

A. Experiments designed to understand flow physics

B. Experiments designed to develop physical models for CFD codes

C. Experiments designed to calibrate CFD codes

D. Experiments designed to validate CFD codes

All four catagories of experiments are important and are necessary to build a mature CFD capability. Validation experiments should only be a part of the total experimental focus and should be formulated to provide specific data for validating CFD codes.

Equally important for validation is the mapping of the CFD code's sensitivity to numerical algorithms, grid density, and physical models. These effects must be known to the same degree as experimental accuracy and resolution in order to understand the applicability of the code over a wide range of flow parameters. This is particular important to the design engineer, who must often rely on computer studies to make a design decision.

CATEGORIES OF CFD–RELATED EXPERIMENTS

A. Experiments designed to understand flow physics

B. Experiments designed to develop physical models for CFD codes

C. Experiments designed to calibrate CFD codes

D. Experiments designed to validate CFD codes

The Ad Hoc Committee on CFD Code Validation
NASA Aeronautics Advisory Committee

CFD CODE VALIDATION DEFINITION

"Detailed surface-and-flow-field comparisons with experimental data to verify the codes ability to accurately model the critical physics of the flow. Validation can occur only when the accuracy and limitations of the experimental data are known and throughly understood and when the accuracy and limitations of the codes numerical algorithms, grid density effects, and physical basis are equally known and understood over a range of specified parameters".

The Ad Hoc Committee on CFD Code Validation
NASA Aeronautics Advisory Committee

BASIC OR BENCHMARK SUBSONIC FLOW PHENOMENON

3D Paraboiized Navier Stokes Analysis

This section, entitled Basic or Benchmark subsonic flow phenomenon, will describe basic subsonic flow interactions that are classic in the sense that they occur in every subsonic bending duct. They are fundamental to the understanding of flow distortion that arises from the development of pressure driven secondary flow and accounts for most of the flow problems that appear at the compressor face. This section will deal with unseparated laminar and turbulent flow. Subsequent sections in this lecture series will deal with "near" and "large" flow separations.

Secondary flow is formed because the fluid near the flow axis of the bending duct, having higher velocity, is acted upon by a larger centrifugal force than the slower fluid near the walls. The faster moving fluid at the center moves outwards, pushing the fluid in the boundary layer at the outer wall (pressure surface) arcurd towards the inner wall (suction surface). Thus fresh fluid is continually being brought into the neighborhood of the outer wall and forced toward the inner wall. The overturning that occurs in the boundary layer generates a strong vortex system, which migrates away from the wall near the bend exit, or compressor face, and is the primary source of flow distortion.

BASIC OR BENCHMARK SUBSONIC FLOW PHENOMENON
3D Parabolized Navier Stokes Analysis

- Development and Evolution of Flow Distortion
- Origins and Effect of Secondary Flow
- Unseparated Laminar and Turbulent Flow

CIRCULAR 90 DEGREE INPLANE BEND

Extensive calculations were made for the flow geometry in which detailed measurements were made by Enayet, Gibson, and Taylor (Ref. 45). This geometry consisted of a 90 degree circular-arc-bend with constant area circular cross sections. The ratio of bend radius to duct diameter was 2.8. The measurements were taken for Reynolds numbers of 790 (laminar flow) and 40,000 (turbulent flow). Two computational grid systems were used for the laminar evaluation; a coarse mesh composed of 20X20X75 (30,000) points and a fine mesh composed of 40X40X75 (120,000) points. On a CRAY I high speed computer, these two cases used 0.7 and 2.9 minutes of CPU time. Likewise, two grid systems were used for the turbrlent cases; a coarse mesh composed of 25X25X86 (53,750) points and a fine mesh having 50X50X86 (215,000) points. Calculations were performed on the Lewis CRAY I computer using a total of 1.3 and 5.1 minutes of CPU time respectively. A comparison between the experimental data and the analysis using the coarse and fine grid systems is presented in the first of two figures for the laminar flow case. Two small regions of "weak" separation were encountered for the laminar flow case. The first separation region was located at the entrance to the bend on the outer wall and the second near the bend exit on the inner wall. A comparison of the measured and computed streamwise velocity profiles show that the "separation model" within the Lewis PNS solver can simulate the effects of "weak" separations on the main flow field. The second figure presents the structure of the secondary flow at the four experimental measuring stations. The secondary flow is formed because the fluid near the flow axis, having higher velocity, is acted upon by a larger centrifugal force than the slower fluid near the walls. The faster moving fluid at the center moves outwards, pushing the fluid in the boundary layer at the outer wall around toward the inner wall. Thus fresh fluid is continually being brought into the neighborhood of the outer wall and forced toward the inner wall. The overturning that occurs in the boundary layer generates a strong vortex system, which migrates away from the wall near the bend exit. Presented in third figure is a comparison between the measured and computed turbulent streamwise velocity profiles at the four measuring stations through the 90 degree bend. For turbulent flow, the results were very sensitive to mesh resolution in the regions of high shear, as can be seen in this figure. The last of the four figure sequence presents the turbulent secondary flow structure which consists of a pair of counter-rotating vortices formed from the overturning of the flow within the wall boundary layer. This "overturning" can also be seen in the surface oil film patterns presented in the last of four figures.

CIRCULAR 90 DEGREE INPLANE BEND
R/r = 3.2, Turbulent Flow, Rey = 40,000
Streamwise Velocity

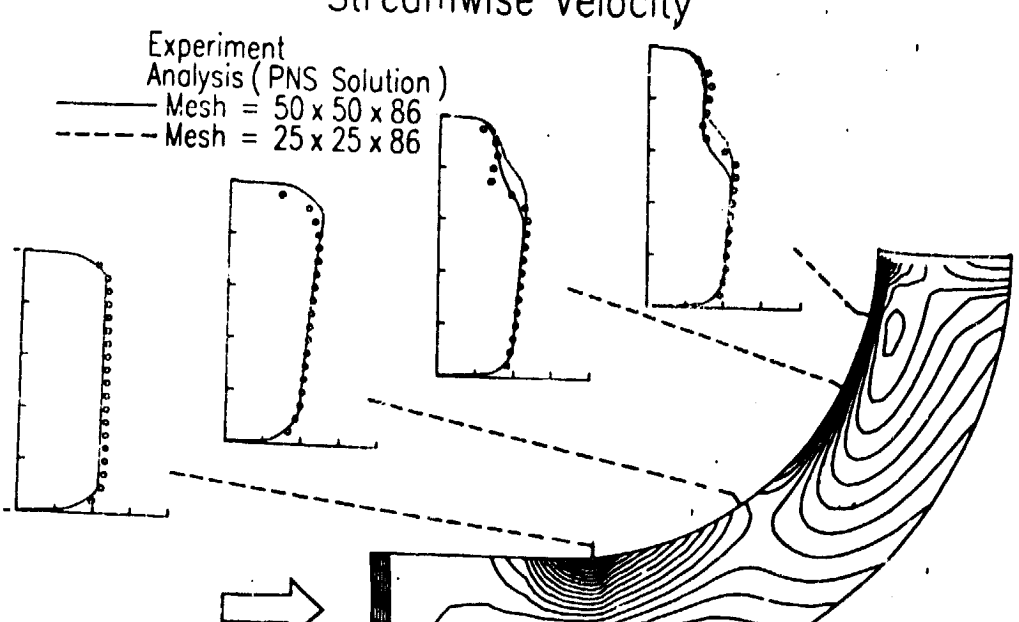

Surface Shear Stress

CIRCULAR 90 DEGREE INPLANE BEND
R/r = 3.2, Turbulent Flow, Rey = 40,000
Secondary Velocity

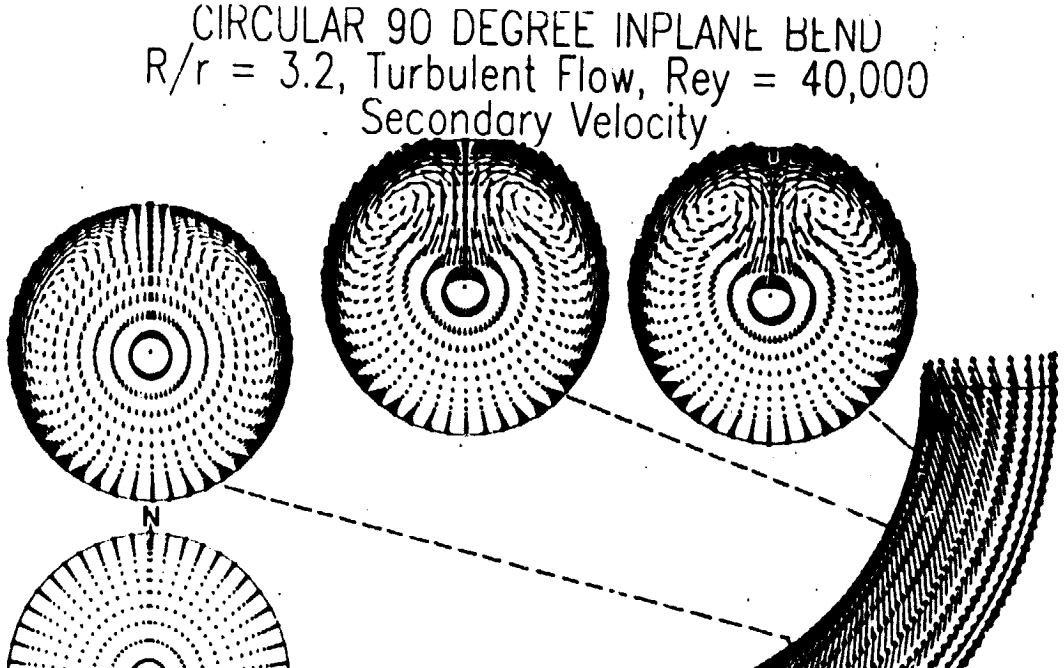

Near Surface Velocity Vectors

CIRCULAR 90 DEGREE INPLANE BEND
R/r = 3.2, Laminar Flow, Rey = 790
Streamwise Velocity

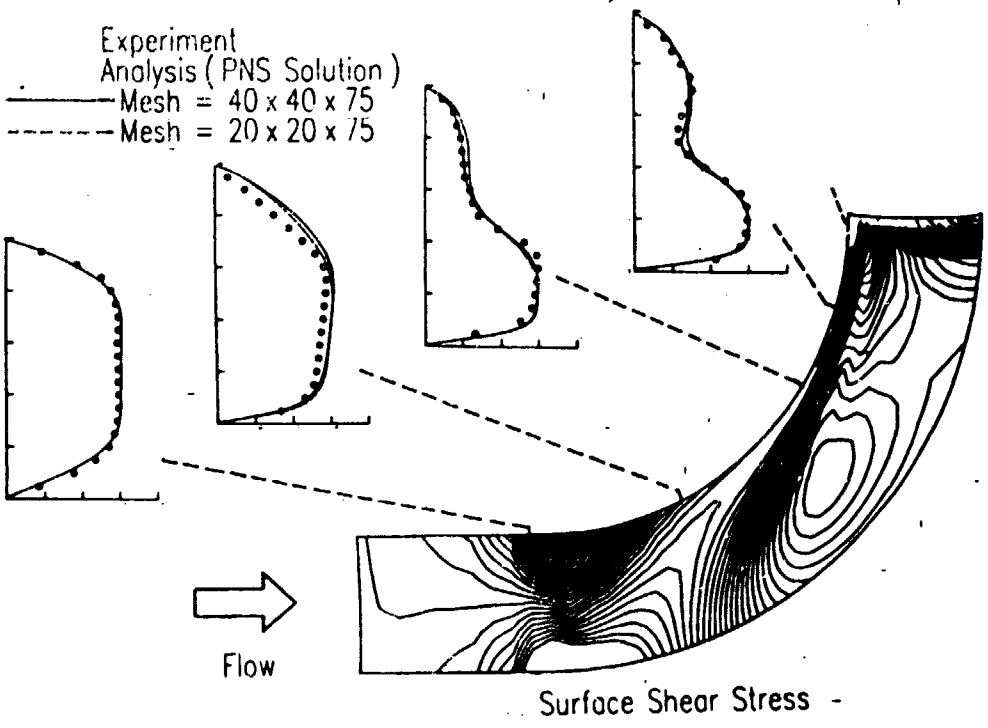

CIRCULAR 90 DEGREE INPLANE BEND
R/r = 3.2, Laminar Flow, Rey = 790
Secondary Velocity

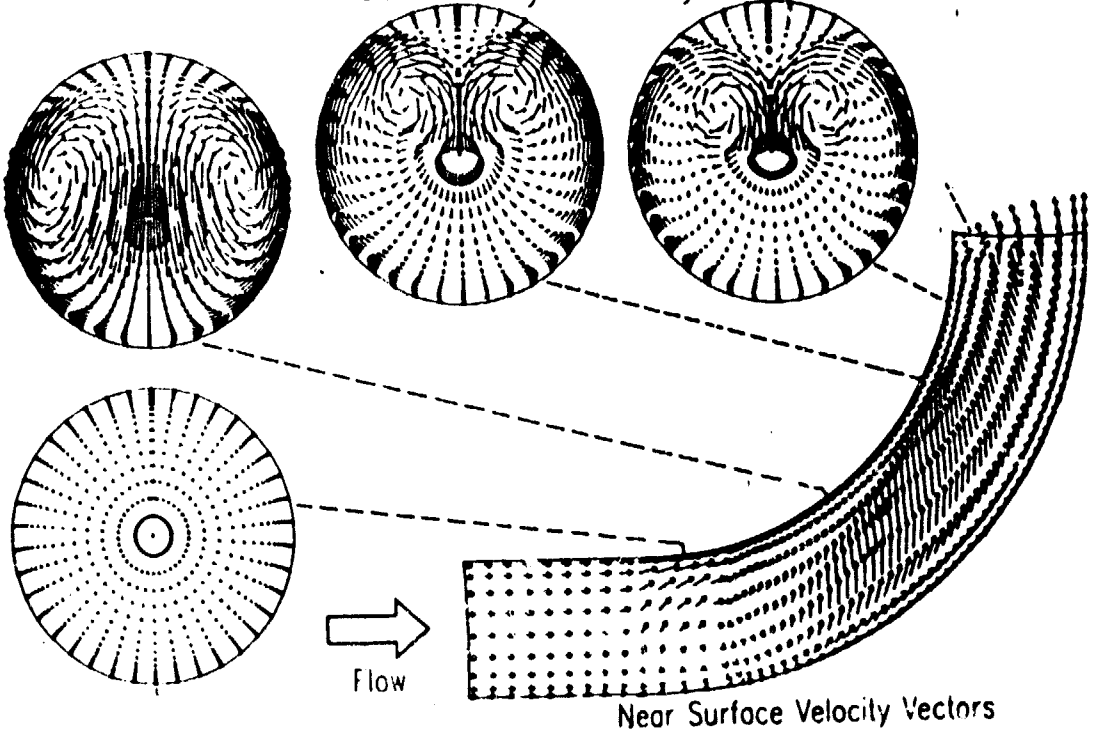

CIRCULAR 180 DEGREE INPLANE BEND

R/r = 20, Laminar Flow, Rey = 1263

Agrawal, Talbot, and Gong (Ref 46) have obtained detailed LDV measurements of laminar flow development in circular 180 inplane bends with uniform entry velocity. This set of experimental data was used by Towne (Ref. 53) to evaluate and verify the ability of the Lewis three dimensional PNS flow solver to quantitatively predict the generation of pressure driven secondary flows in curved ducts. Experimental data were obtained at a Reynolds number of 1263, based on the cross sectional radius and entery velocity. The Dean number was 565. A computational mesh consisting of 50X50 points in the half transverse plane and 226 forward marching steps, for a total of 565,000 mesh points, was used for the results shown in this figure. On a CRAY I computer, this calculation took 17 minutes of CPU time. A comparison between the measured and calculated streamwise contour plots presented in this figure demonstrates that for well prescribed geometry description and initial data, the Lewis PNS solver can simulate the fine detail of flow structure associated with developing pressure driven flow fields.

CIRCULAR 180 DEGREE INPLANE BEND
R/r = 20, Laminar Flow, Rey = 1263
PNS Solution, Theta = 84 degrees
Mesh = 50 X 50 X 226 = 5.65×10^5

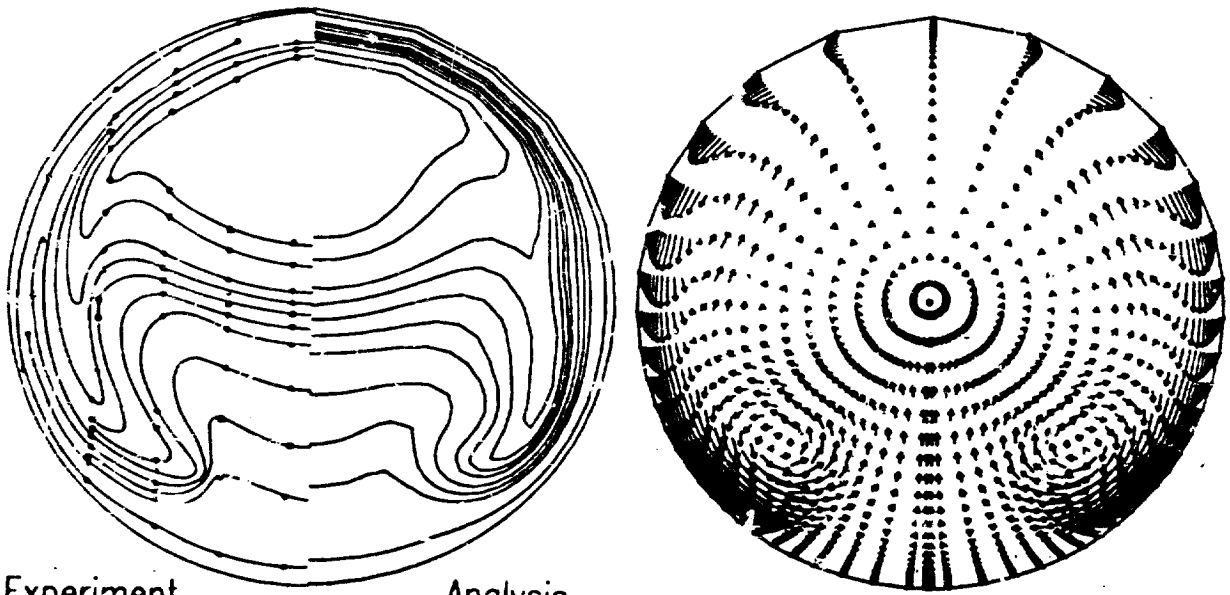

Experiment Analysis

Streamwise Velocity Secondary Velocity

CIRCULAR 180 DEGREE INPLANE BEND

R/r = 7, Laminar Flow, Rey = 242

Towne (Ref. 53) also evaluated the Lewis PNS viscous flow solver using the experimental results of Agrawal, Talbot, and Gong (Ref. 46) for the R/r=7 duct configuration. Shown on these figures are the computed secondary velocity vectors and the measured v-component of velocity along the dotted reference lines. Comparisons were made at survey stations of Theta=15.0, 50.0, 75.0, 105.0, and 135.0 degrees. These calculations were performed at a Reynolds number of 242, based on the cross section radius r and entry velocity. The dean numbver was 183.

The computations were made with a 20x20 mesh in the half section (taking advantage of symmetry), and 181 streamwise marching steps, using 1.7 minutes of CPU time on a CRAY-1 computer. This series of figures clearly shows the structure of the pressure driven secondary flow development and is a classical pattern for flow in curved ducts.

CIRCULAR 180 DEGREE INPLANE BEND
R/r = 7, Laminar Flow, Rey = 242
PNS Solution, Secondary Flow
Theta = 15.0 degrees

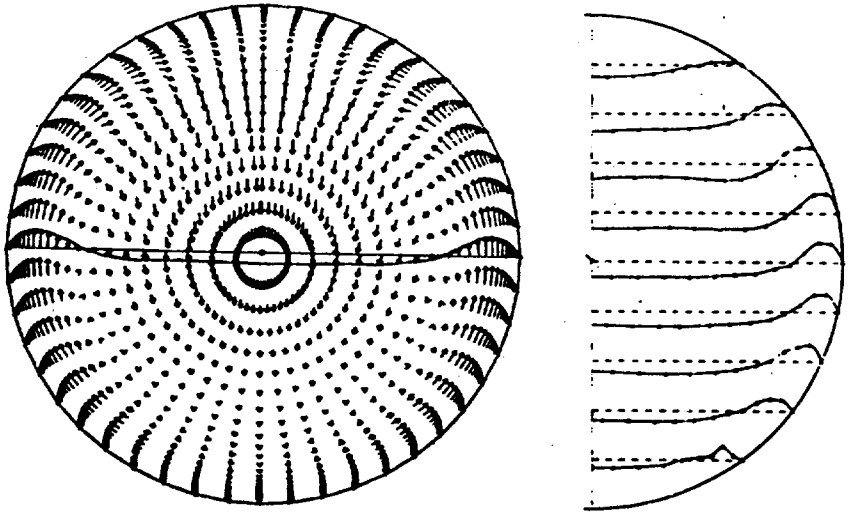

Analysis

Experiment

CIRCULAR 180 DEGREE INPLANE BEND
R/r = 7, Laminar Flow, Rey = 242
PNS Solution, Secondary Flow
Theta = 50.0 degrees

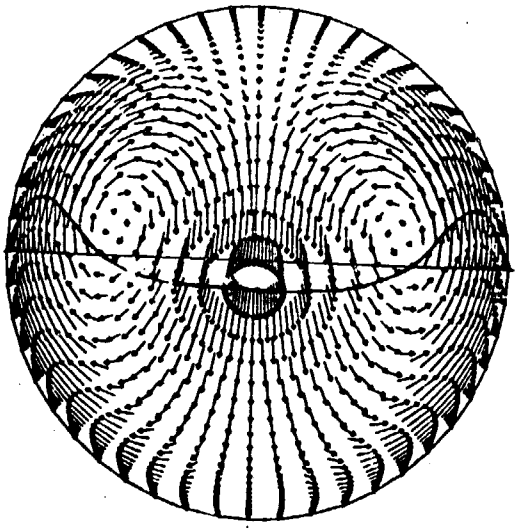

Analysis

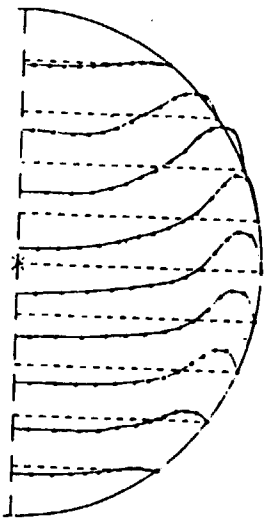

Experiment

CIRCULAR 180 DEGREE INPLANE BEND
R/r = 7, Laminar Flow, Rey = 242
PNS Solution, Secondary Flow
Theta = 75.0 degrees

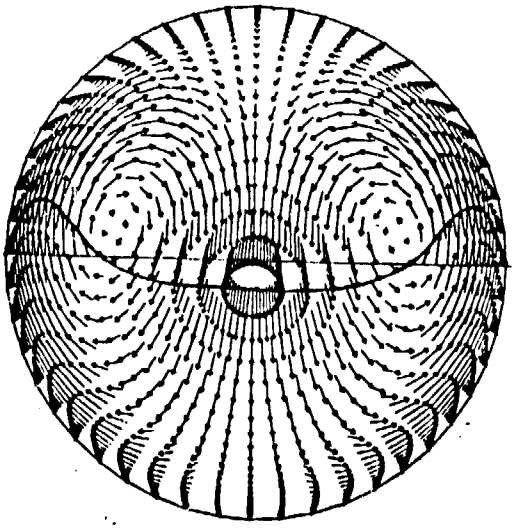

Analysis

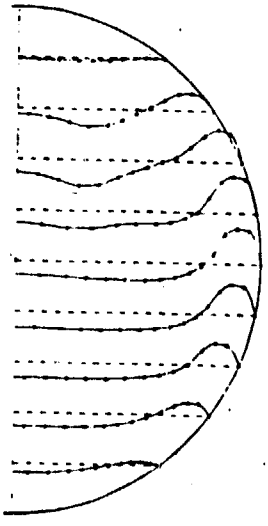

Experiment

CIRCULAR 180 DEGREE INPLANE BEND
R/r = 7, Laminar Flow, Rey = 242
PNS Solution, Secondary Flow
Theta = 105.0 degrees

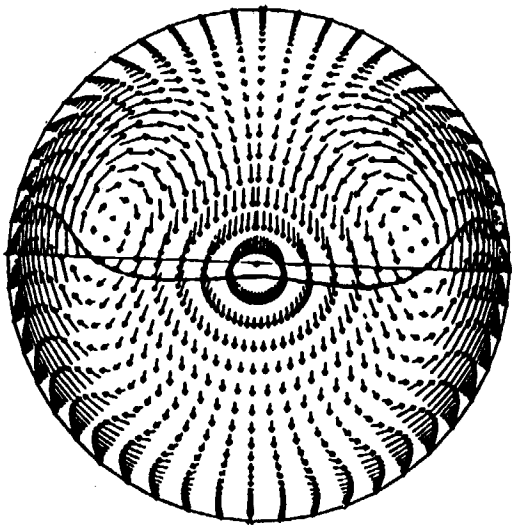

Analysis

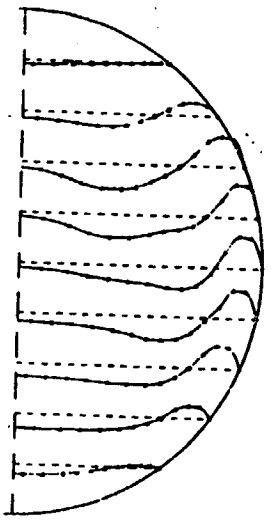

Experiment

CIRCULAR 180 DEGREE INPLANE BEND
R/r = 7, Laminar Flow, Rey = 242
PNS Solution, Secondary Flow
Theta = 135.0 degrees

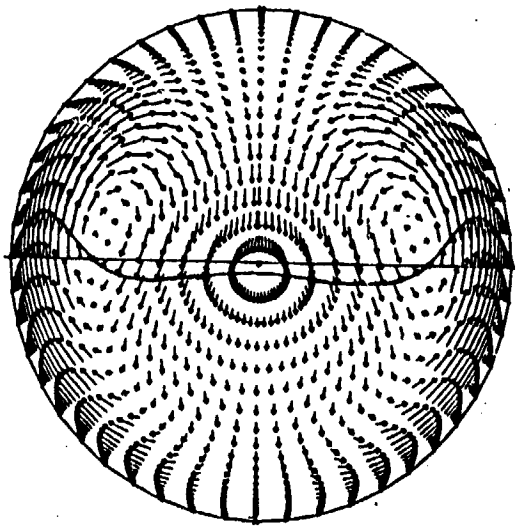

Analysis

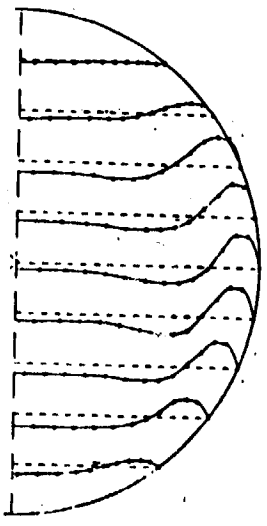

Experiment

CIRCULAR 22.5-22.5 DEGREE INPLANE S-BEND

Taylor, Whitelaw and Yianneskis (Ref. 48), in an experimental investigation sponsored by NASA Lewis Research Center, obtained a series of 3-component LDV velocity measurements on the structure of the flow that develops in a 22.5-22.5 degree circular S-bend. Measurements were made in laminar flow at a Reynolds number of 790 and turbulent flow at a Reynolds number of 48,000. Two computational grid systems were used for the laminar evaluation; a coarse mesh system composed of 20X20X80 (32,000) points and a fine mesh system composed of 40X40X80 (128,000) points. On a CRAY I computer, these two cases used 0.8 and 3.0 minutes of CPU time. Likewise, two mesh systems were used for the turtbulent cases; a coarse mesh composed of 25X25X80 (50,000) points and a fine mesh system of 50X50X80 (200,000) points. Calculations were performed on a CRAY I computer using a total of 1.2 and and 4.8 minutes of CPU time respectively. The first figure of this four figure sequence shows a comparison between the measured and computed laminar development of streamwise velocity profiles at the four measurement stations through the S-duct. Because the boundary layers were large relative to the duct dimensions, the laminar flow calculations were not sensitive to mesh resolution. The complex secondary flow structure that can develop in S-duct configurations is graphically shown in the second figure. The system of counter rotating vortices develops in the first bend and in the second bend, the secondary flow begins to reverse forming another pair of counter rotating vortices. Much greater sensitivity to resolution of high shear regions was encountered for the turbulent flow development through the S-duct, as shown on the third figure. Qualitatively, the turbulent flow development resembles the laminar field; however, the high Reynolds number in the turbulent results in less severe secondary flow, as shown on the last figure. Again, the computed results are in very good agreement with experiment for both the laminar and turbulent cases, (Ref. 47).

CIRCULAR 22.5 – 22.5 DEGREE INPLANE S-BEND
Laminar Flow, Rey = 790
Streamwise Velocity

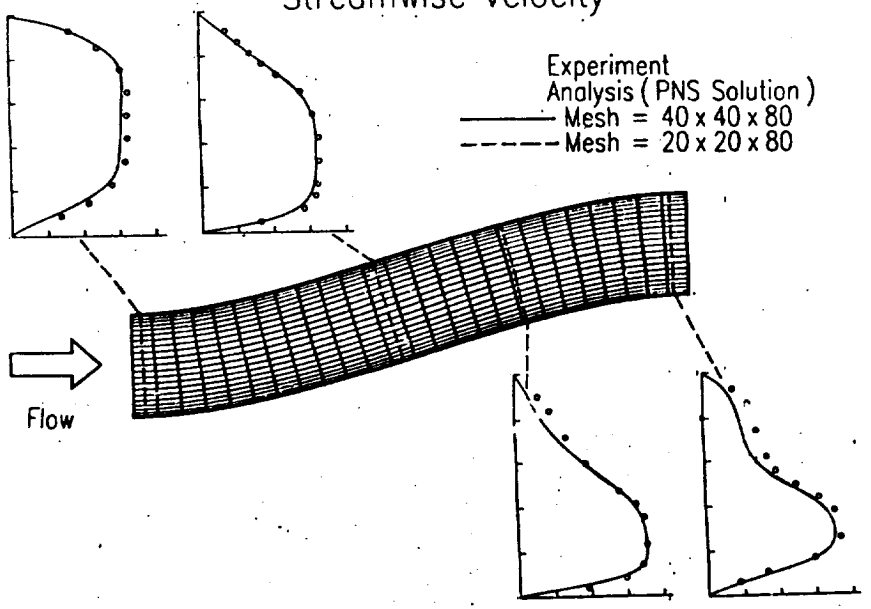

CIRCULAR 22.5 – 22.5 DEGREE INPLANE S-BEND
Laminar Flow, Rey = 790
Streamwise Velocity

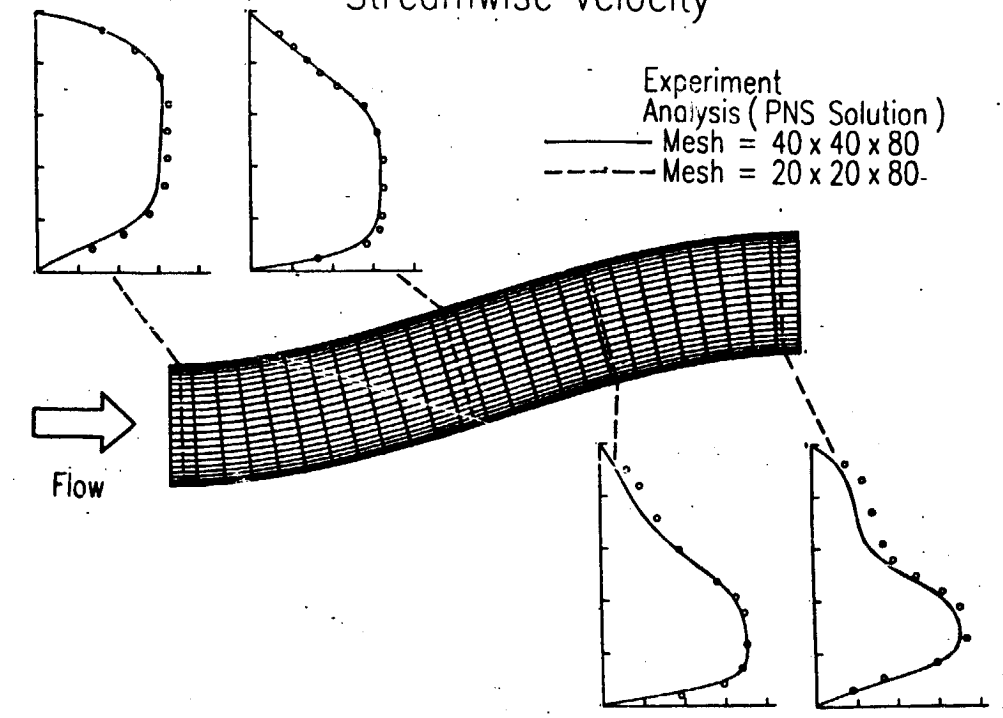

CIRCULAR 22.5 – 22.5 DEGREE INPLANE S-BEND
Laminar Flow, Rey = 790
Secondary Velocity

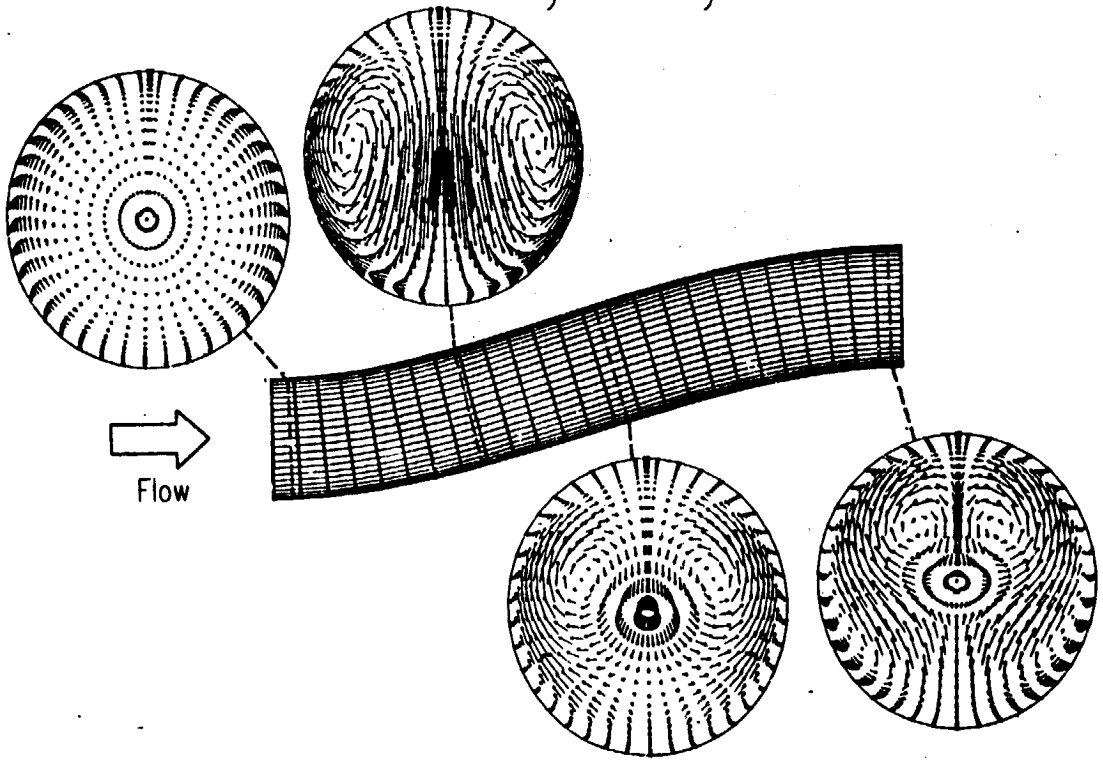

CIRCULAR 22.5 – 22.5 DEGREE INPLANE S–BEND
Turbulent Flow, Rey = 48,000
Streamwise Velocity

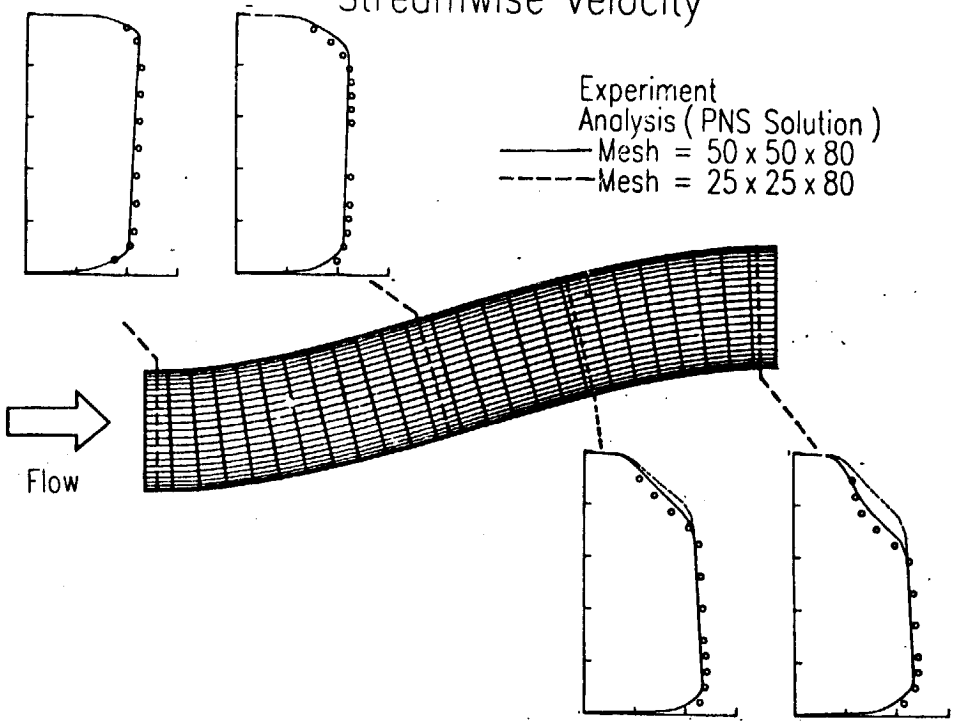

CIRCULAR 22.5 – 22.5 DEGREE INPLANE S–BEND
Turbulent Flow, Rey = 48,000
Secondary Velocity

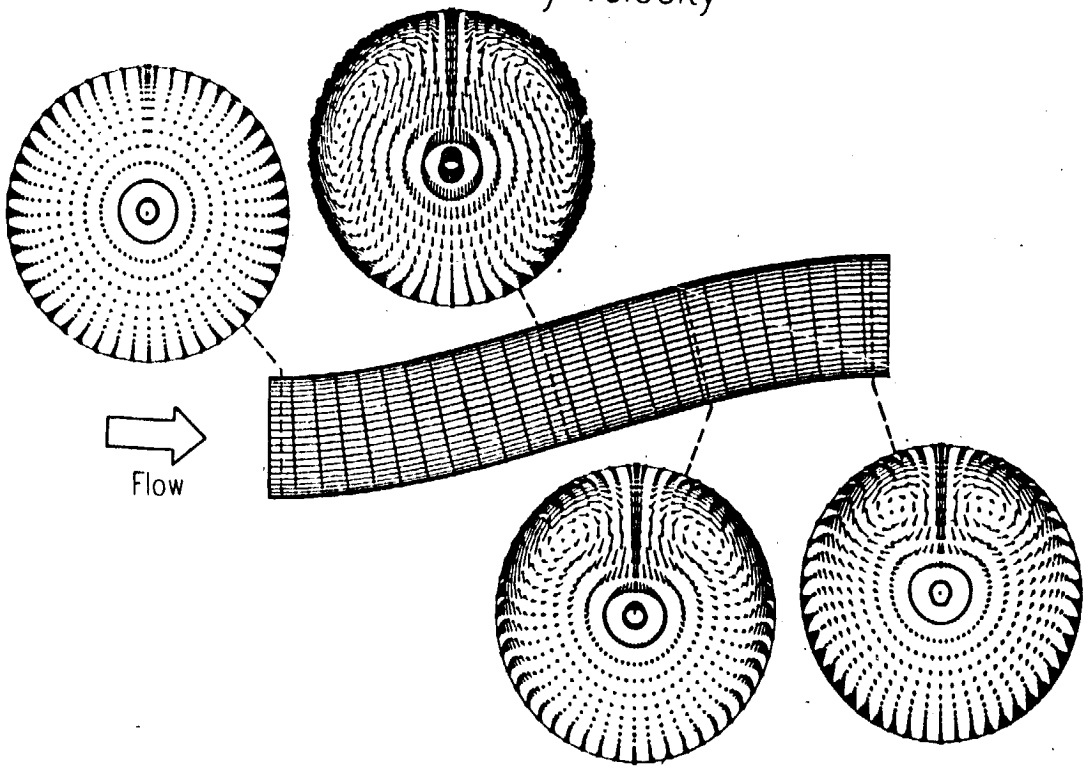

BASIC OR BENCHMARK SUBSONIC FLOW PHENOMENON

3D Parabolized Navier Stokes Analysis

The second section in this lecture on "CFD Application to Inlet Airframe Integration" deals with the analysis of duct flows at higher entrance Mach number and Reynolds number, typical of "real world" conditions. At these conditions separation is more likely to occur and thus the ability to compute such flows is more uncertain because of turbulence models.

BASIC OR BENCHMARK SUBSONIC FLOW PHENOMENON
3D Parabolized Navier Stokes Analysis

- Inlet Duct Flow Distortion
- "Small" and Confined Flow Separation

CIRCULAR 45-45 DEGREE INPLANE S-BEND

Vinf = 45 m/sec, Turbulent Flow, Rey = 5.0x10e6

A series of measurements obtained at the Department of Aeronautics, Imperial College of Science and Technology, by Bansod and Bradshaw (Ref 49) were used to verify the Lewis PNS solver at higher Reynolds numbers. The configuration used for this study was the 45-45 symmetric, short intake, S-shaped duct with an R/D of 2.25. The duct entry velocity was nominally set at 45 meters/sec, which gave a Reynolds number of 5.0E5 based on duct diameter. Measurements were presented of total pressure, static pressure, surface shear stress, and yaw angle for the flow through the S-shaped duct. The computational mesh used for this study was 50X50X100, for total of 250,000 mesh points. Computations were performed on a CRAY I high speed computer using 6.0 minutes of CPU time. Shown on the first figure in a series of three figures is a comparison between the calculated and measured surface shear stress at three circumferential surface lengths labeled the N-length, E-length, and S-length. Excellent agreement was obtained in spite of the fact that a simple eddy viscosity turbulence model was used in this calculation. Shown in the second figure is the surface shear stress color signature for this S-shaped duct. The small region of separation or near separation that was observed by Bansod and Bradshaw along the N-length is clearly visible from the wall shear stress signature. The last figure in this sequence of three figures shows a comparison between the calculated and measured total pressure loss contours at the compressor face station in addition to the secondary velocity vector flow field. It is clear that the Lewis PNS three dimensional flow solver captured the proper flow physics at the compressor face including the pair of counter-rotating vortices in the boundary layer, (Ref. 49).

CIRCULAR 45–45 DEGREE INPLANE S–BEND
Vinf = 45 m/sec, Turbulent Flow, Rey = 5.0×10^6
Surface Shear Stress

CIRCULAR 45 – 45 DEGREE INPLANE S–BEND
PNS Solution, Surface Skin Friction
Turbulent Flow, Rey = 5.0×10^5

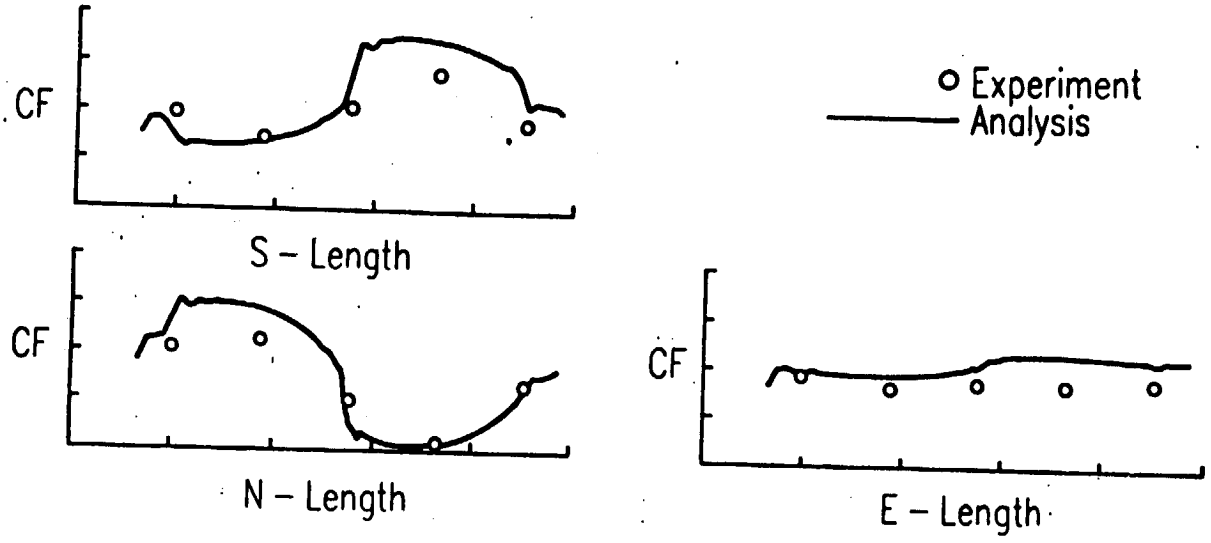

CIRCULAR 45 – 45 DEGREE INPLANE S–BEND
PNS Solution, Compressor Face Station
Turbulent Flow, Rey = 5.0×10^5

Mesh = $50 \times 50 \times 100 = 2.5 \times 10^5$

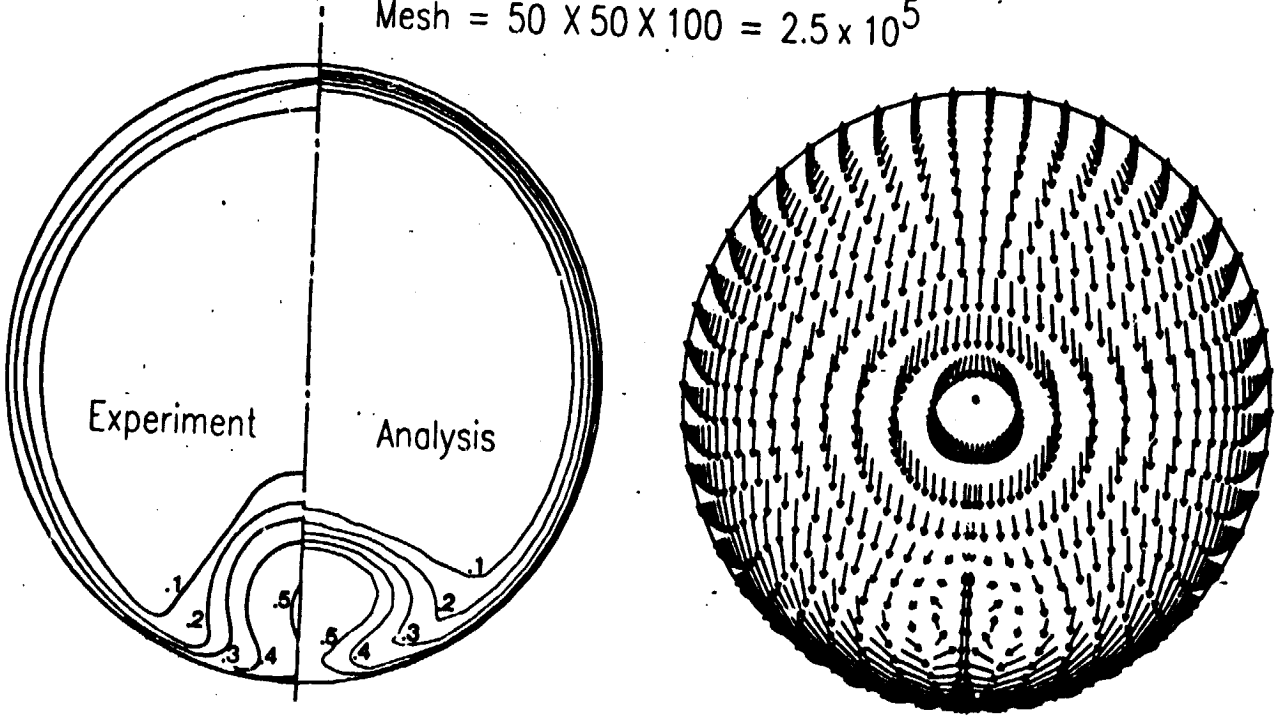

Total Pressure Loss

Secondary Velocity

UNIVERSITY OF TENNESSEE INLET DUCT

Circular 30-30 degree Inplane S-Bend

Aexit/Ainlet=1.0, Minf=0.6, Rey=1.76x10e6

This series of figures describes experimental measurements and comparision with computations performed using the Lewis Parabolized Navier Stokes code within a constant circular cross section 30-30 degree S-duct. The experimental and computational results by Vakili, Wu, Bhat, Liver, Kingst, and Towne are reported in Ref. (51), and was sponsored by the NASA Lewis Research Center under a university grant. The 30-30 degree circular cross section S-duct, shown on this figure, was made from two symmetric sections. The duct inside diameter D was 16.51 cm and the mean radius of curvature R was 83.82 cm. Upstream of this duct section, a 76.20 cm straight pipe was installed to allow for the development of the turbulent boundary layer to the desired thickness. At the downstream exit, the S-duct was attached to another pipe of length 152.40 cm.

All the measurments were made at a nominal free stream Mach number of 0.60 at the reference measurment station in the straight section X=24.8 cm. The flow parameters at thius point were used as reference conditions for non-dimensionalizing the data. The Reynolds number at this station was 1.76x10e6, and the boundary layer thickness was 0.64 cm.

Measurements were made using a five port cone probe, which was traversed along a radial direction at ten azimuthal angles 20 degrees apart. Wall static pressures were also measured along the duct at azimuthal angles of 0, 90, and 180 degrees.

UNIVERSITY OF TENNESSEE INLET DUCT
Circular 30–30 degree Inplane S–Bend
Aexit/Ainlet = 1.0, Minf = 0.6, Rey = 1.76×10^6

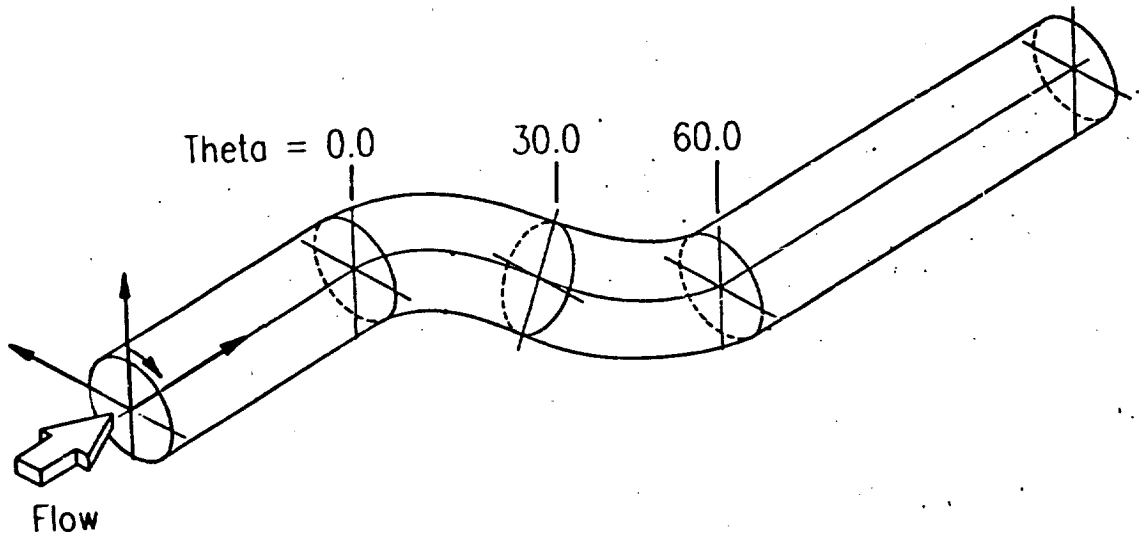

UNIVERSITY OF TENNESSEE INLET DUCT

Circular 30-30 degree Inplane S-Bend

Total Pressure Contours

Aexit/Ainlet=1.0

Analysis of the cone probe data resulted in determination of total and static pressure values as well as local velocity vectors. Six stations were traversed. These included one station in the straight seccion upstream of the duct entrance at X/D=-1.5, and stations at theta=2.0, 15.0, 32.0, 45.0 and 60.0 degrees. At each station a total of ten radial traverses were made on both sides of the symmetry plane.

The total pressure contours at four stations are shown on this figure, with the experimental results on the left half and the computational results on the right half of each section. The region of low kinetic energy in the second bend is particularly clear on these figures. In the first bend the "inviscid" core is initially moved towards the inner wall and then towards the outer wall in the junction of the first and second bends. The flow enters the second bend with the core deflected towards the inner wall. Experimental and calculated contours of total pressure show mainly the resulting distortion effects of pressure-driven secondary flows in this S-bend. Both the experiment and analysis show a large low pressure zone near the outer wall of the second bend. The computations appear to be underpredicting this total pressure distortion, which could be the influence of the turbulence model, which does not include wall curvature effects.

Surface oil flow visualization in the region of the inflection point indicates the existence of a region where the flow appears to be nearing separation. However the ability to calculate close to the region of "near" or "small" separations is particularly sensitive to the turbulence model. In general, the flow studied was dominated by pressure forces rather than shear forces, hence the influence of stress driven flows may be small and the effective viscosity approach may be appropriate. Stll, consideration should be given to stress-based turbulence models.

UNIVERSITY OF TENNESSEE INLET DUCT
Circular 30-30 degree Inplane S-Bend
Total Pressure Contours
Aexit/Ainlet = 1.0

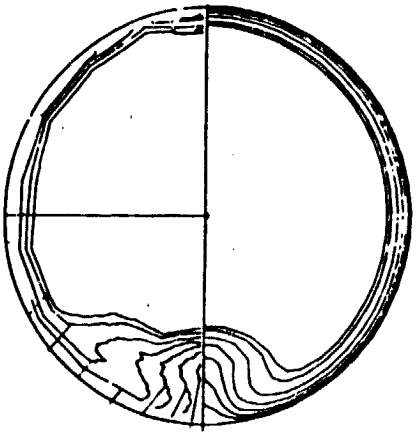

Experiment Analysis
Theta = 45.0 degrees

Experiment Analysis
Theta = 60.0 degrees

UNIVERSITY OF TENNESSEE INLET DUCT
Circular 30-30 degree Inplane S-Bend
Total Pressure Contours
Aexit/Ainlet = 1.0

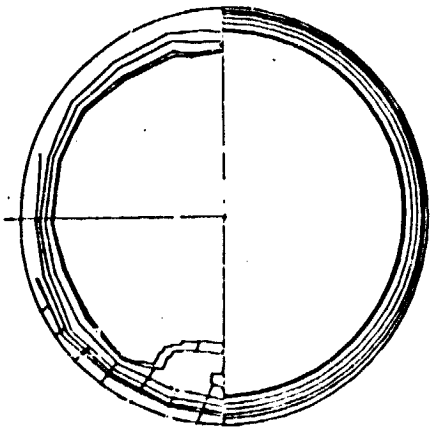

Experiment Analysis
Theta = 15.0 degrees

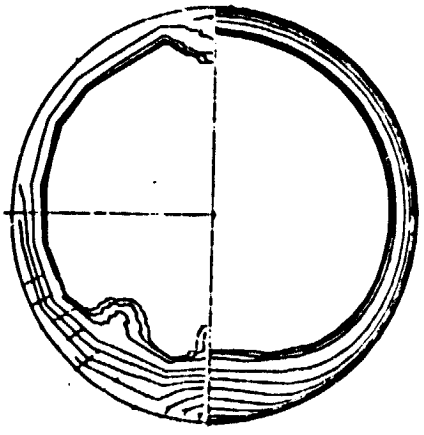

Experiment Analysis
Theta = 32.0 degrees

BASIC OR BENCHMARK SUBSONIC FLOW PHENOMENON

3D Parabolized Navier Stokes Analysis

This last section deals with the analysis of a class of flows in which large and confined separation are present, and/or where vortex generators are used to control the separation process. The analysis of these flows are sensitive to the turbulence model, particularly with regards to the separation boundaries and overall duct losses. Separated flow often include large-scale unsteadyness. If the computation is to represent the average flow, the turbulence model must include the effect of this unsteadiness. These structures and the transport that they produce are strongly influenced by such effects as flow curvature, and these effects must also be included in the turbulence model.

BASIC OR BENCHMARK SUBSONIC FLOW PHENOMENON
3D Parabolized Navier Stokes Analysis

- High Inlet Duct Flow Distortion
- "Large" and Confined Flow Separation
- Vortex Generator Flows

ROYAL AIRCRAFT ESTABLISHMENT

Series 2129 Aircraft Intake Ducts

The next two figures are different views of two generic ducts used in a joint NASA/RAE research program on intake duct flows. These intake ducts were studied experimentally by RAE, and computationally by NASA at Lewis Research Center using the Lewis 3D Parabolized Navier-Stokes code. Both intake ducts had circular cross-sections and an area ratio of 1.4. The flow was turbulent, with inlet Mach numbers that ranged from 0.395 to 0.794 and Reynolds numbers (based on inlet diameter and flow conditions) from 3.9 to 6.6 million.

ROYAL AIRCRAFT ESTABLISHMENT
Series 2129 Aircraft Intake Ducts
Geometry Definition

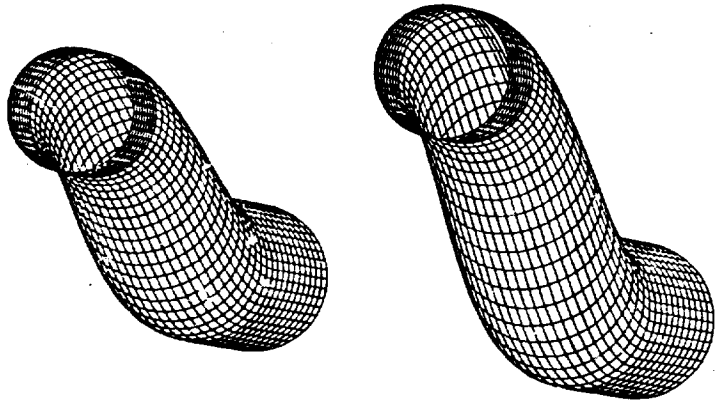

Offset/Length = 0.30 Offset/Length = 0.45

ROYAL AIRCRAFT ESTABLISHMENT
Series 2129 Aircraft Intake Ducts
Geometry Definition

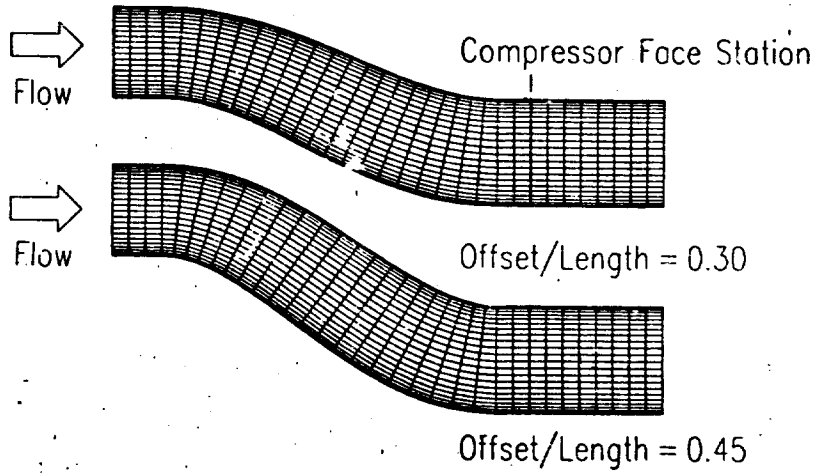

RAE2129 AIRCRAFT INTAKE DUCT

Compressor Face Total Pressure

The next several figures present computational and experimental results, in the form of constant total pressure contours at the compressor face station, for both ducts at different flow conditions. The distortion in the flow, evident by the concentration of low total pressure at the bottom of the duct, is typical of S-duct intakes. The level of distortion increases with inlet Mach number and, as one would expect, with the amount of offset. In general the agreement between the computational and experimental results is good, especially for the lower offset case. It should be noted that the computations do not include the effect of the compressor face hub.

RAE2129 AIRCRAFT INTAKE DUCT
Compressor Face Total Pressure
Offset/Length = 0.30, M = 0.608, Re = 5.61×10^6

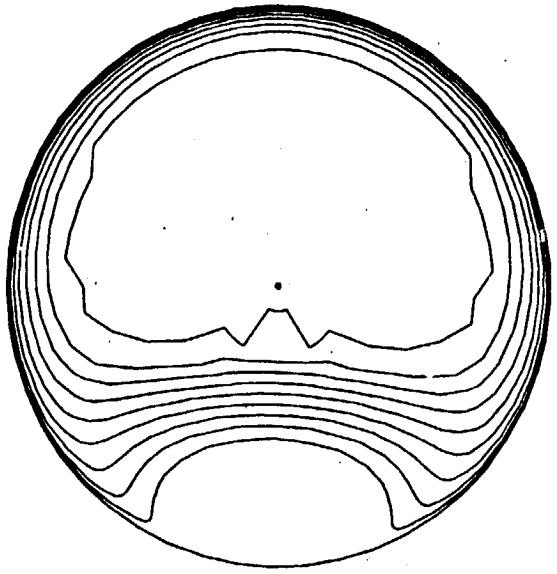

Analysis (No Hub)

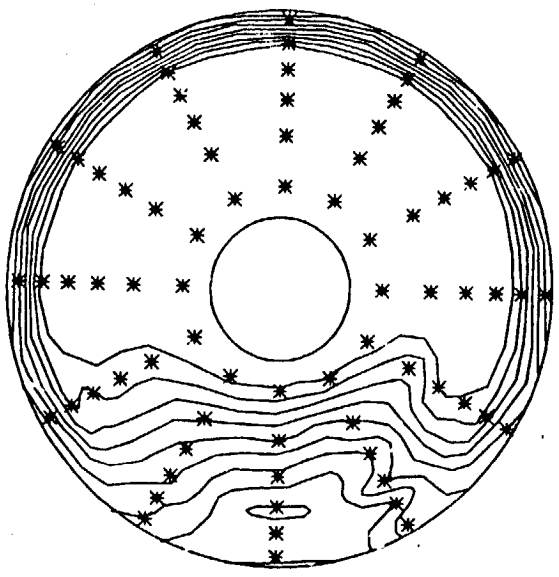

Experiment

RAE2129 AIRCRAFT INTAKE DUCT
Compressor Face Total Pressure
Offset/Length = 0.30, M = 0.412, Re = 4.13×10^6

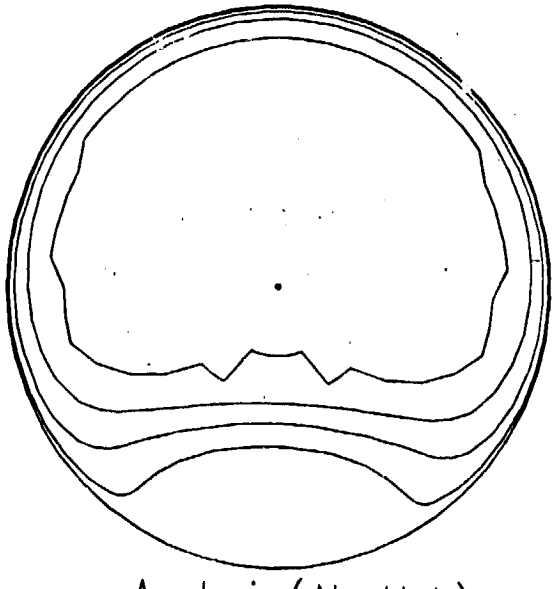

Analysis (No Hub)

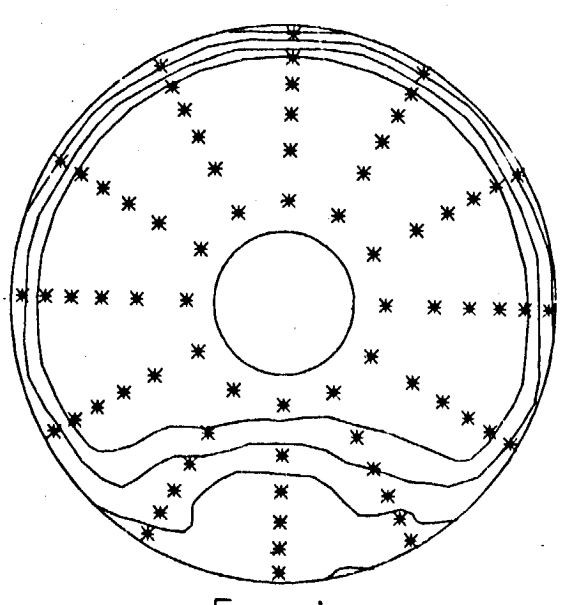

Experiment

RAE2129 AIRCRAFT INTAKE DUCT
Compressor Face Total Pressure
Offset/Length = 0.30, M = 0.794, Re = 6.60×10^6

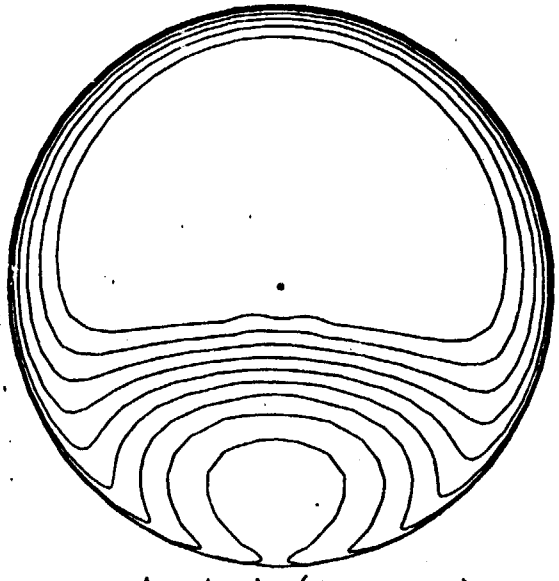

Analysis (No Hub)

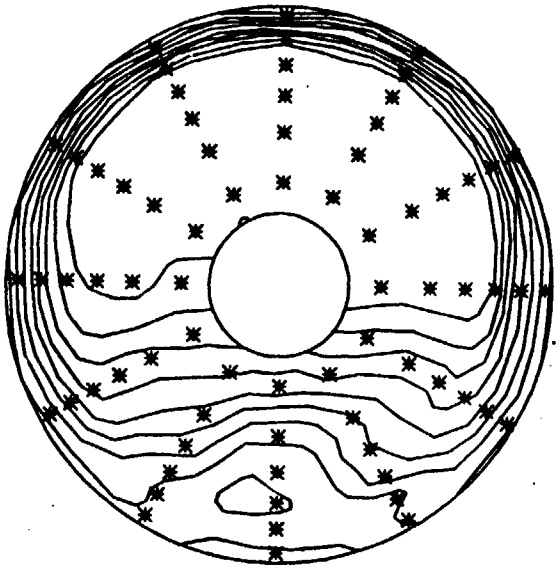

Experiment

RAE2129 AIRCRAFT INTAKE DUCT
Compressor Face Total Pressure
Offset/Length = 0.45, M = 0.385, Re = 3.90×10^6

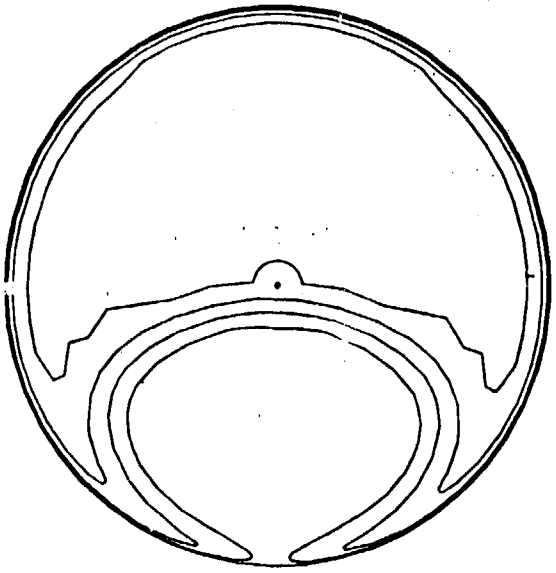

Analysis (No Hub)

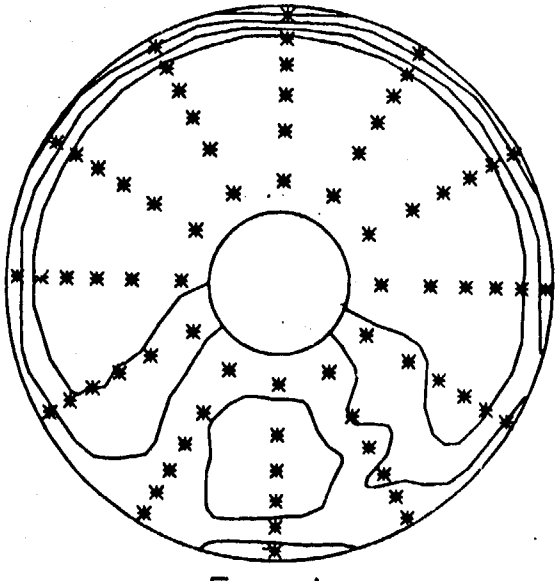

Experiment

RAE2129 AIRCRAFT INTAKE DUCT
Compressor Face Total Pressure
Offset/Length = 0.45, M = 0.773, Re = 6.50×10^6

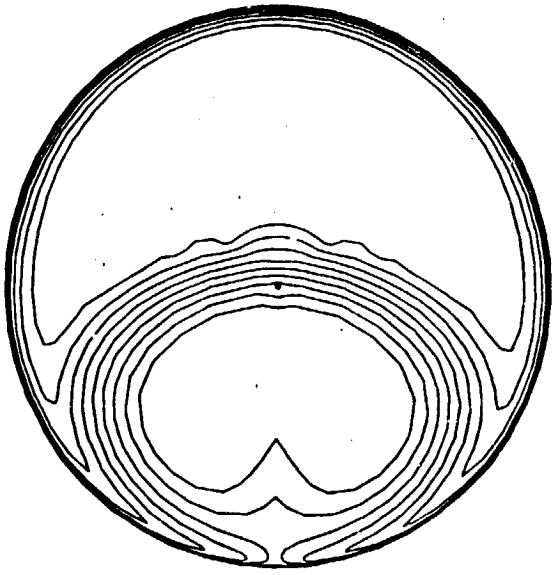

Analysis (No Hub)

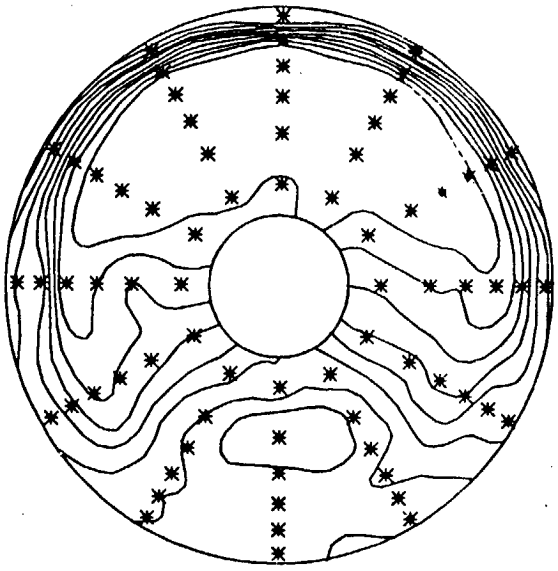

Experiment

RAE2129 AIRCRAFT INTAKE DUCT
Compressor Face Total Pressure
Offset/Length = 0.45, M = 0.573, Re = 5.37×10^6

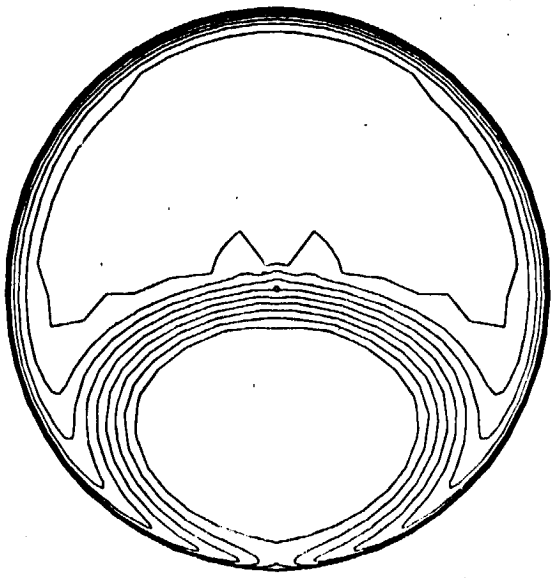

Analysis (No Hub)

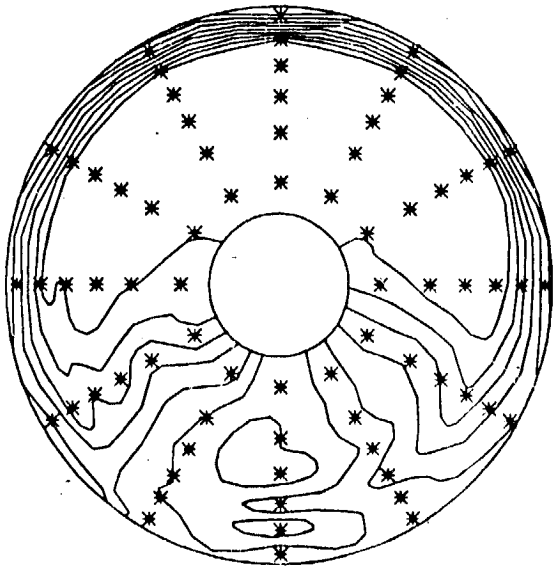

Experiment

RAE2129 AIRCRAFT INTAKE DUCT

Compressor Face Secondary Velocity Vectors

Minf = 0.78, Rey = 6.5x10e6

The distortion patterns shown in the previous figures are the result of secondary flows in the S-duct. In this figure the computed secondary velocity vectors (i.e., the velocity vectors normal to the duct centerline) are shown at the compressor face station for both intakes at the highest Mach number that was run. The length of the reference vector at the bottom of the figure corresponds to 0.1 times the inlet velocity.

These secondary flows are the result of pressure gradients due to the S-duct curvature. In the first bend, the high pressure at the outside of the bend drives the low energy boundary layer toward the inside, while the core flow responds to centrifugal effects and moves toward the outside. The result is a pair of counter-rotating secondary flow vortices. In the second bend, the direction of the cross-flow pressure gradients reverses. However, the flow enters the second bend with a vortex pattern already established. The net effect is to tighten and concentrate these vortices near the bottom of the duct, in agreement with classical secondary flow theory.

RAE2129 AIRCRAFT INTAKE DUCT
Compressor Face Secondary Velocity Vectors
M = 0.78, Rey = 6.5×10^6

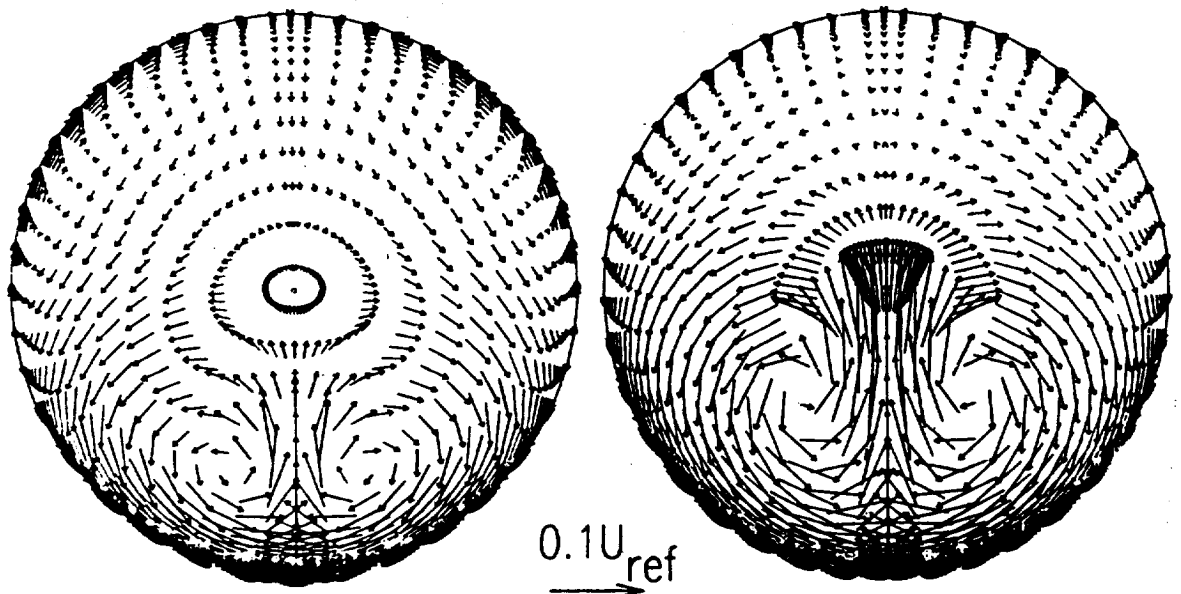

Offset/Length = 0.30 Offset/Length = 0.45

RAE2129 AIRCRAFT INTAKE DUCT

Streamwise Velocity Contours in Vertical Plane

Minf = 0.78, Rey = 6.5x10e6

In this figure, computed constant streamwise velocity contours are shown in the duct symmetry plane for both S-ducts. The distortion development described previously can also be seen in this figure. It should be noted that, in both ducts, a separation bubble was predicted along the bottom of the duct around the inflection station between the two bends. The low-velocity flow, which has begun to accumulate in this region, is unable to negotiate the local adverse pressure gradient caused by the change in wall curvature from convex to concave. The PNS analysis was able to march through this region using the FLARE approximation.

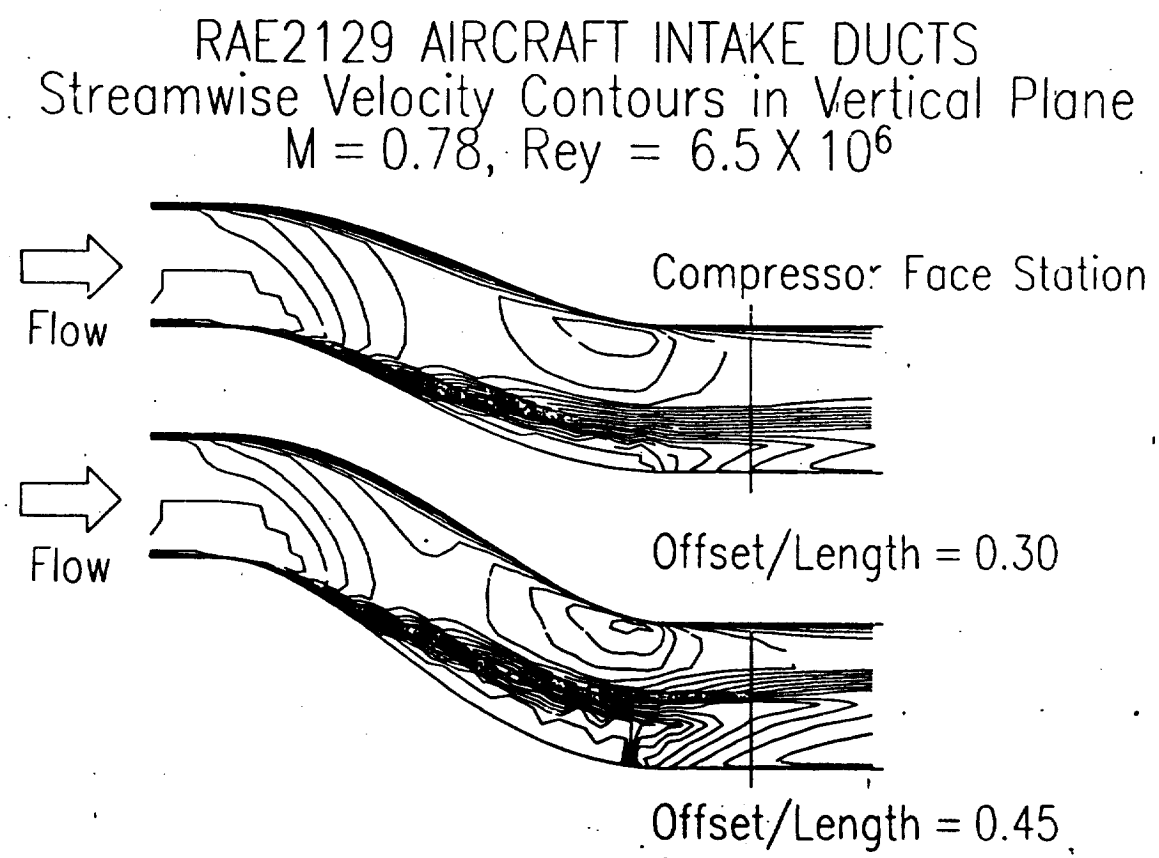

UNIVERSITY OF TENNESSEE INLET DUCT

Circular 30-30 degree Inplane S-Bend

Aexit=1.5, Minf=0.6, Rey=1.76x10e6

Vakili, Wu, Liver, and Bhat (Ref. 56) in an experimental investigation sponsored by NASA Lewis Research Center obtained a series of measurements in a 30-30 degree diffusing S-duct of area ratio 1.5 with and without vortex generators. The flow in this duct was turbulent with a Mach number of 0.6 and Reynolds number based on inlet duct diameter of 1.76x10e6. In both the experiment and analysis the flow in the duct separated. This was due to the adverse pressure gradient of the area change in combination with the effect of pressure driven secondary flow due to local centerline curvature. The Lewis PNS solver marches through the separated region by using the "flare" type approximation described in the previous lecture. It must be pointed out that the computed results in the separated region will not be correct because of the "flare" approximations use in the Lewis PNS solver. However the global effects of the separation on the main flow development will be modeled, and it is the purpose of this study to evaluate how well this is accomplished.

UNIVERSITY OF TENNESSEE INLET DUCT
Circular 30–30 degree Inplane S–Bend
Aexit/Ainlet = 1.5, Minf = 0.6, Rey = 1.76×10^6

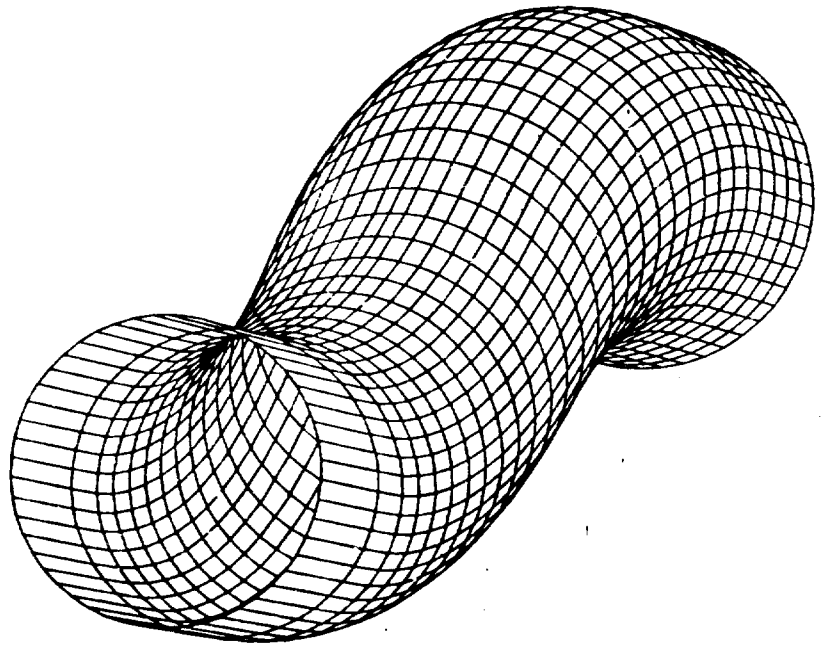

UNIVERSITY OF TENNESSEE INLET DUCT

Validation Survey Stations

No Vortex Generators

The experimental and computational survey stations are shown on this figure, and correspond to X/D=0.0, 1.29, 2.49, 3.70 and 5.00. At each survey station, a five port cone probe was traversed radially at ten azimuthal angles, approximately 20 degrees apart, on both sides of the symmetry plane. At least seventy points were measured at each traverse.

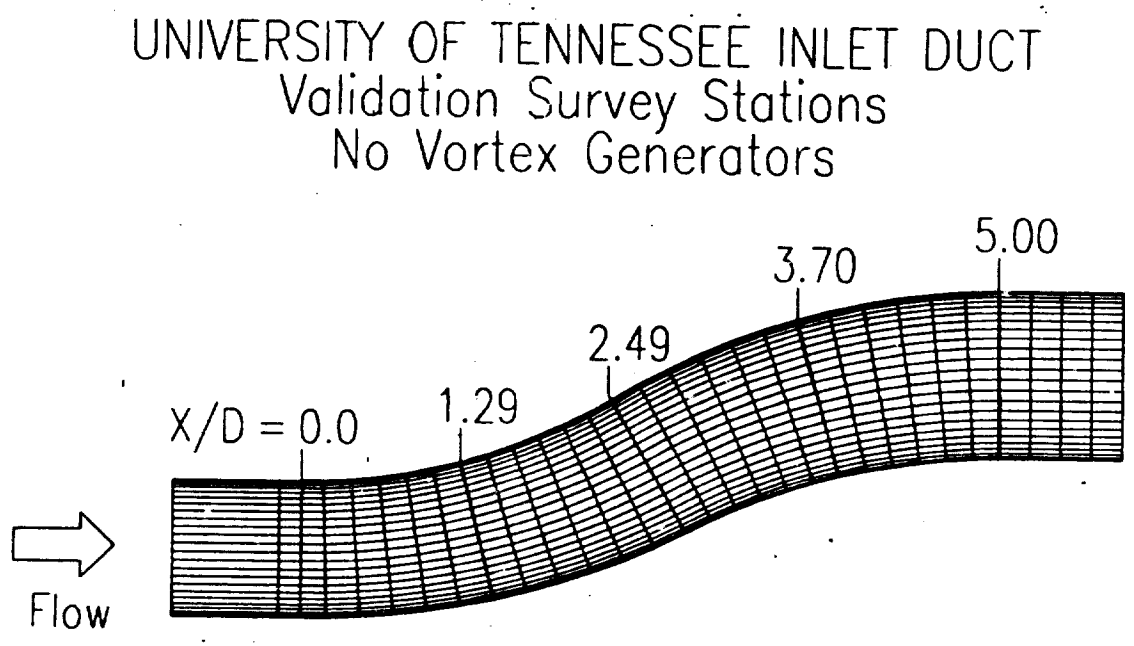

UNIVERSITY OF TENNESSEE INLET DUCT

Circular 30-30 degree Inplane S-Bend

Total Pressure Contours, No Vortex Generators

The following five figures show a comparision of the computed and experimental total pressure coefficient at the survey stations shown on the previous figure. The computed results are on the left side and the experimenal results are on the right. At the second station, the experimental results indicate a large and well developed separation, while the analysis shows only the onset of flow separation. Thus, the computations indicated that the separation bubble was located futher downstream than was indicated by the experimental data.

UNIVERSITY OF TENNESSEE INLET DUCT
Circular 30-30 degree Inplane S-Bend
Total Pressure Contours, No Vortex Generators
X/D = 0.0

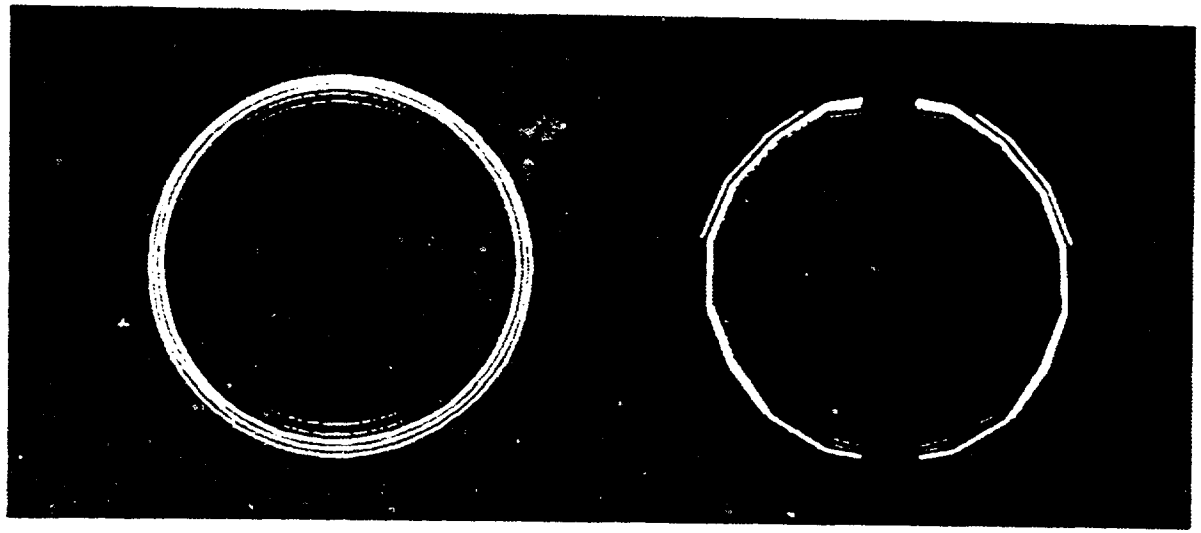

Analysis Experiment

UNIVERSITY OF TENNESSEE INLET DUCT
Circular 30-30 degree Inplane S-Bend
Total Pressure Contours, No Vortex Generators
X/D = 1.29

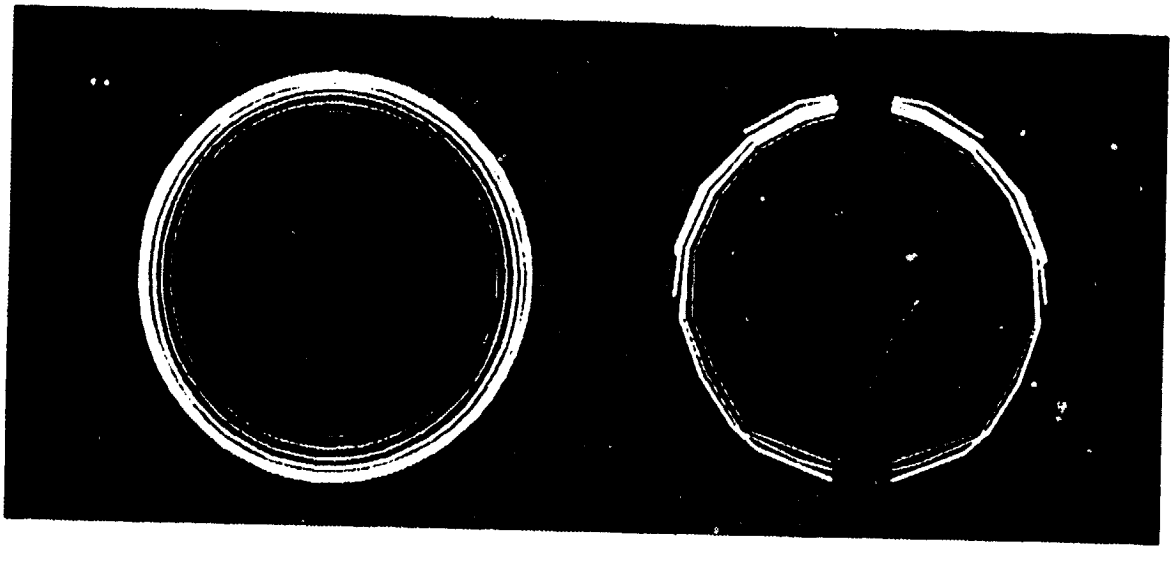

Analysis Experiment

UNIVERSITY OF TENNESSEE INLET DUCT
Circular 30-30 degree Inplane S-Bend
Total Pressure Contours, No Vortex Generators
X/D = 2.49

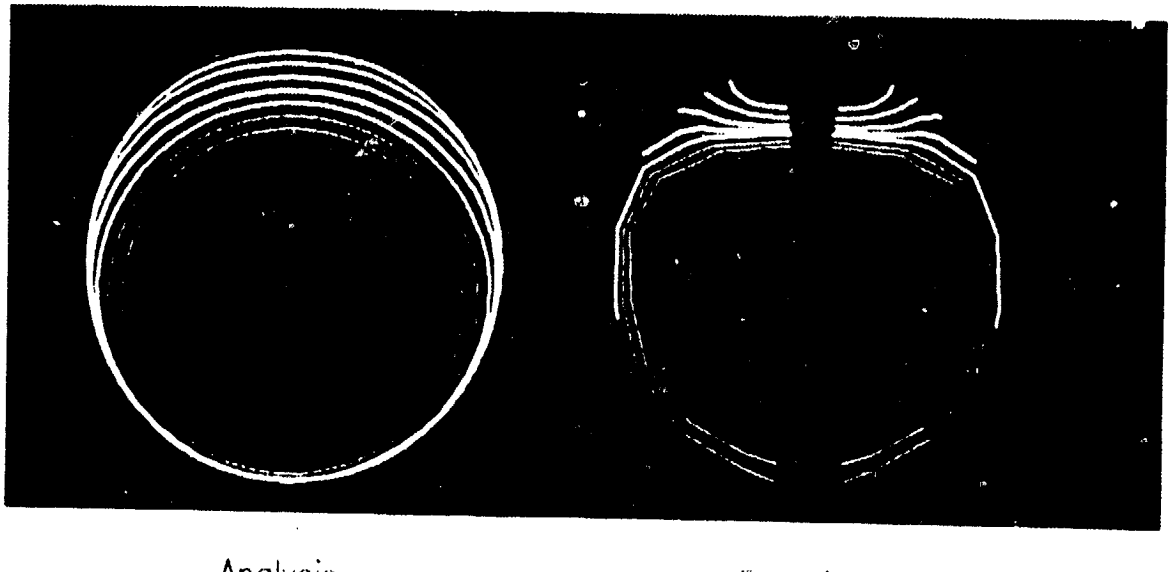

Analysis Experiment

UNIVERSITY OF TENNESSEE INLET DUCT
Circular 30–30 degree Inplane S–Bend
Total Pressure Contours, No Vortex Generators
X/D = 3.70

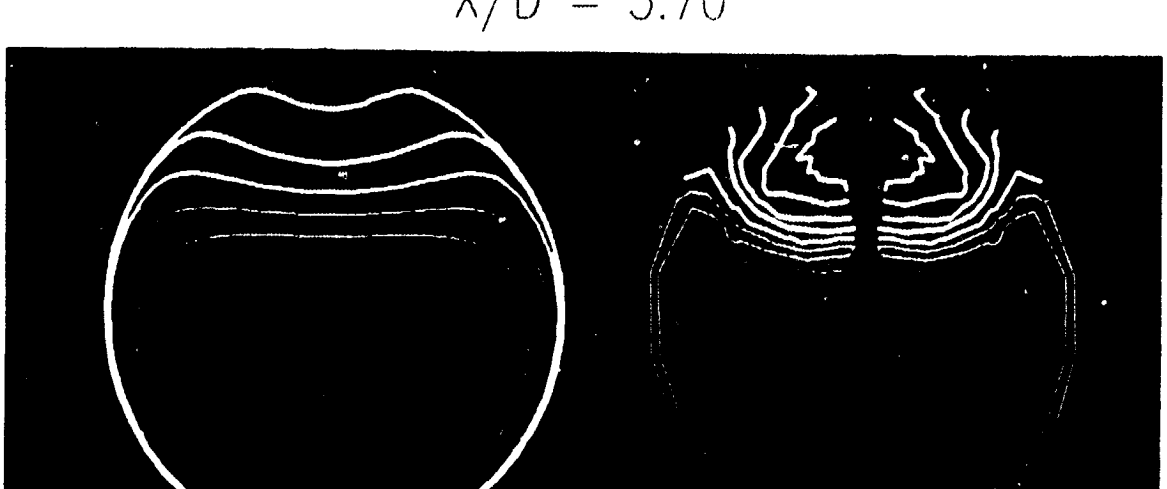

Analysis Experiment

UNIVERSITY OF TENNESSEE INLET DUCT
Circular 30–30 degree Inplane S–Bend
Total Pressure Contours, No Vortex Generators
X/D = 5.00

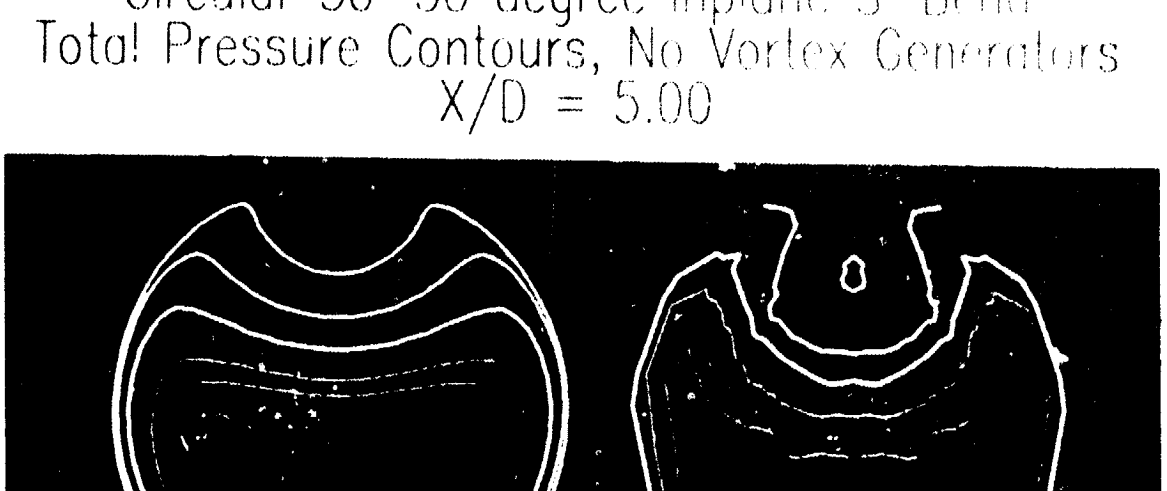

Analysis Experiment

UNIVERSITY OF TENNESSEE INLET DUCT

Experimental Oil Flow Separation Pattern

The three dimensional separation present in the 30-30 degree diffuser S-duct was very severe. As mentioned, the centrifugal forces acting on the flow results in the secondary flow which in turn results in the accumulation of the boundary layer near the inner wall in the first section. The thick boundary layer there is especially susceptible to separation because of the adverse pressure gradient caused by the reverse curvature of the second section. This is a classic situation which will always occur within S-shaped ducts. The core flow moving towards the outer bend through the first section does not follow the curvature in the second section because of the effective change of geometry due to the flow separation.

UNIVERSITY OF TENNESSEE INLET DUCT
Experimental Oil Flow Patterns
Confined Flow Separation

UNIVERSITY OF TENNESSEE INLET DUCT

Validation Survey Stations

Vortex Generators

Because of flow separation that was encountered in the 30-30 degree diffusing S-duct, vortex generator devices were placed in the duct at X/D=0.09, and measurements made at the same survey stations as the previous case, i.e., X/D=0.0, 1.29, 2.49, 3.70, and 5.0. At each survey station, the cone probe was traversed radially at ten azimuthal angles, approximately 20 degrees apart on both sides of the symmetry plane.

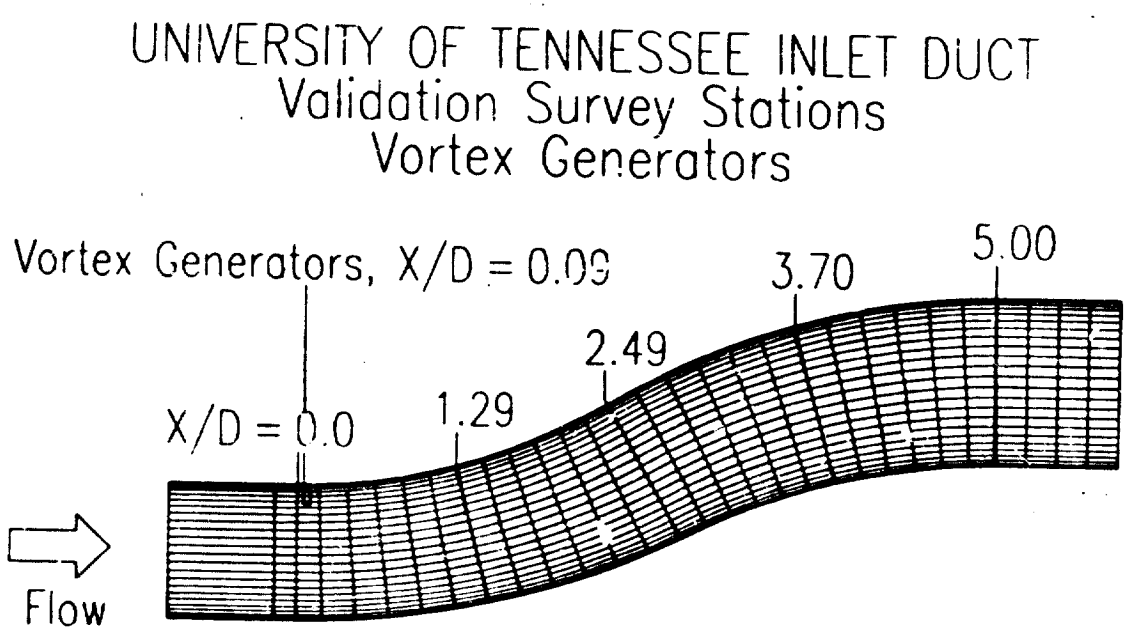

UNIVERSITY OF TENNESSEE INLET DUCT

Location of Vortex Generators

X/D = 0.09

Three pairs of vortex generators were placed in the 30-30 diffusing S-duct at at incidence angles of plus and minus 16 degrees located at azimuthal angles of of -38.0, 0.0, and 38.0 degrees, as shown in this figure.

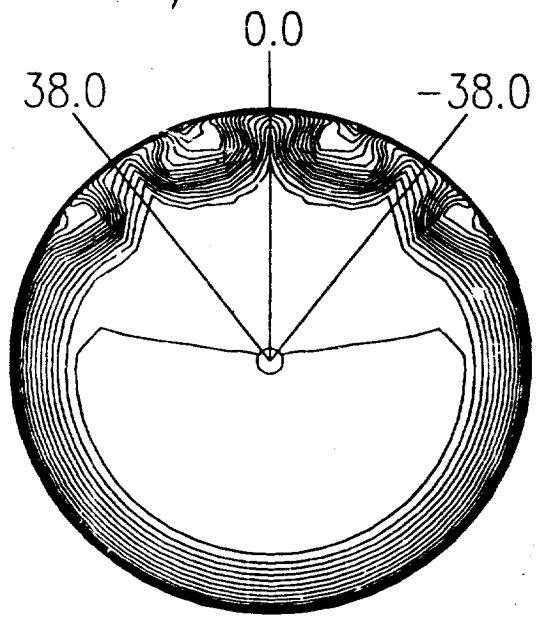

UNIVERSITY OF TENNESSEE INLET DUCT

Circular 30-30 degree Inplane S-Bend

Total Pressure Contours, Vortex Generators

The next five figures show a comparision between the analysis, presented on the left side of each figure, and the experiment, shown on the right side. AT X/D=1.29, the effect of the vortex generators is quite apparent on the total pressure contours. At the five survey stations, the analysis agreed qualitativley with the experimentally measured total pressure contours. In both the computed and measured total pressure contours, the distortion caused by the vortex generators is "pushed" towards the outside of the first bend, opposed to the pressure driven secondary flow induced by the first bend. In comparing the total pressure levels between the separated case and the vortex generator case, it is apparent that the vortex generator devices sucessfully mixed the high energy flow with the low energy flow to suppress separation. In general, the interaction between the induced vortex flow and pressure driven secondary flow that was computed was physically realistic. However, there is a great deal of development that must take place in the analysis if quantitative agreement is to be realized, particularly with the turbulence model.

UNIVERSITY OF TENNESSEE INLET DUCT
Circular 30-30 degree Inplane S-Bend,
Total Pressure Contours, Vortex Generators
X/D = 0.0

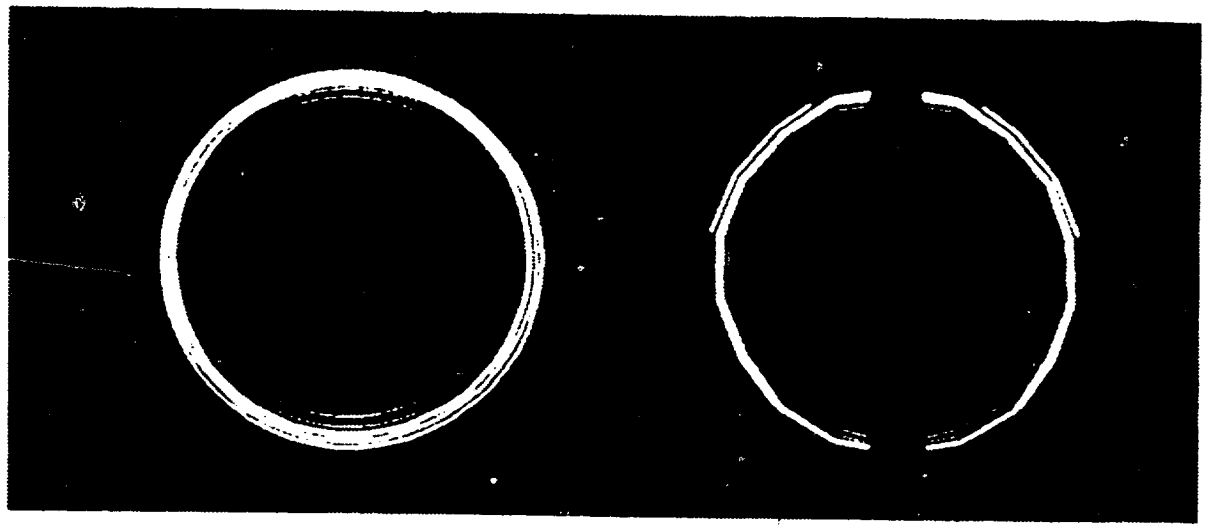

Analysis Experiment

UNIVERSITY OF TENNESSEE INLET DUCT
Circular 30–30 degree Inplane S–Bend
Total Pressure Contours, Vortex Generators
X/D = 1.29

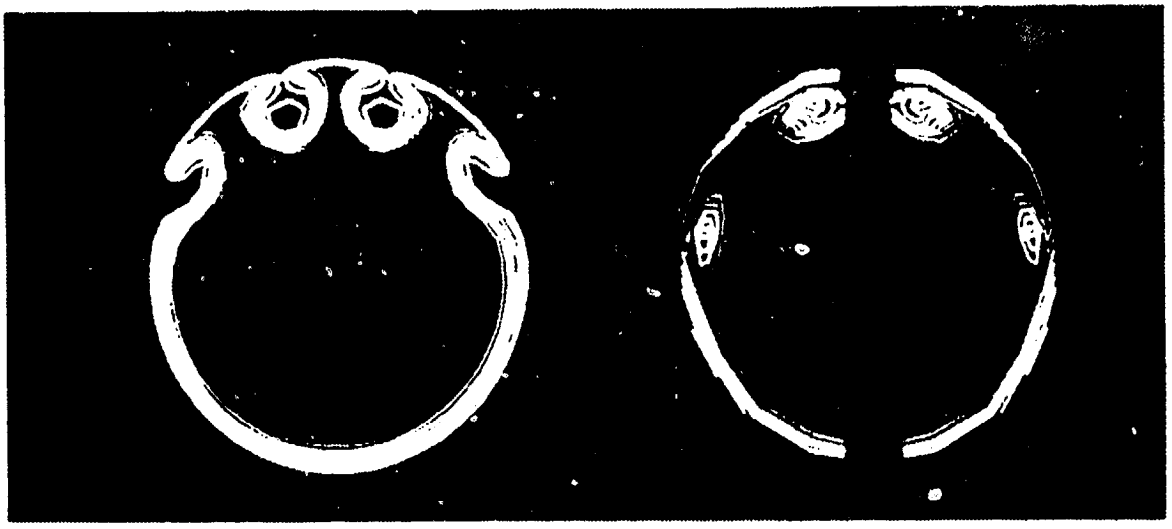

Analysis Experiment

UNIVERSITY OF TENNESSEE INLET DUCT
Circular 30–30 degree Inplane S–Bend
Total Pressure Contours, Vortex Generators
X/D = 2.49

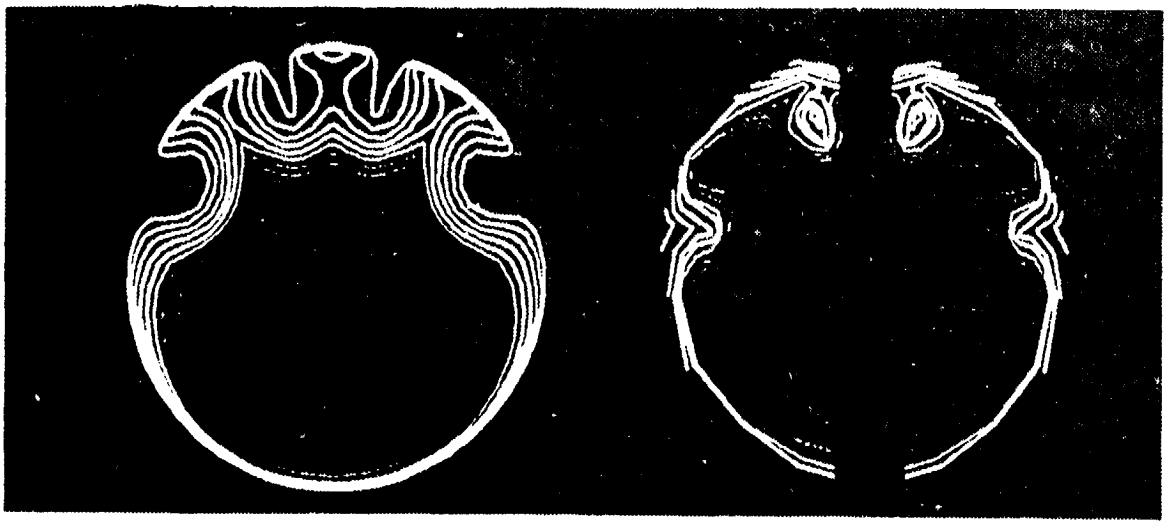

Analysis Experiment

UNIVERSITY OF TENNESSEE INLET DUCT
Circular 30–30 degree Inplane S–Bend
Total Pressure Contours, Vortex Generators
X/D = 3.70

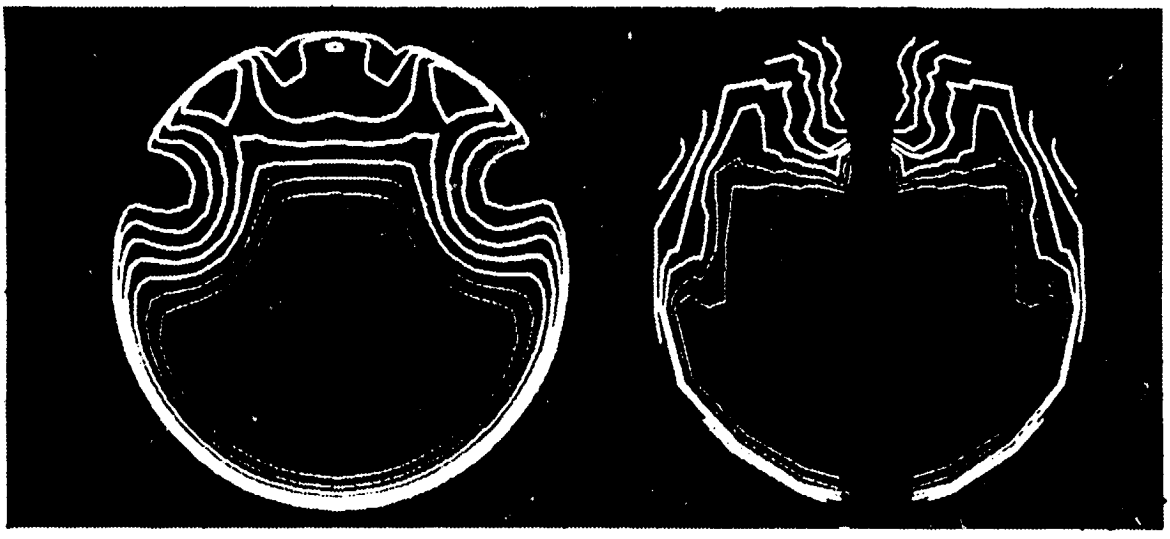

Analysis Experiment

UNIVERSITY OF TENNESSEE INLET DUCT
Circular 30–30 degree Inplane S–Bend
Total Pressure Contours, Vortex Generators
X/D = 5.00

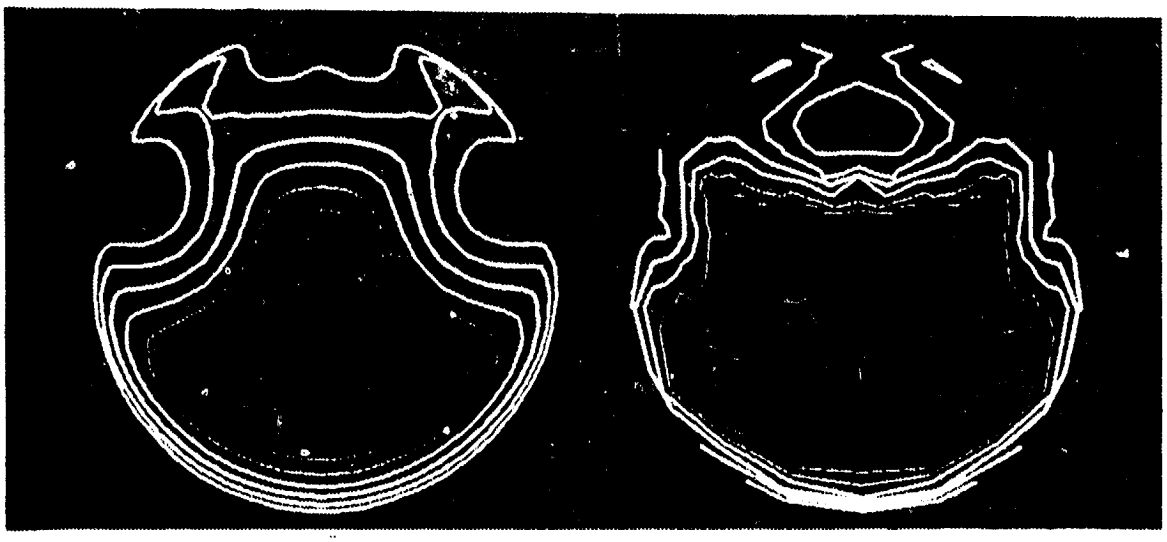

Analysis Experiment

3D SUBSONIC INLET DIFFUSER DUCTS

Boundary Layer Control Techniques

There have been a number of tests to investigate the effect on three-dimensional offset diffuser performance of a wide variety of wall blowing concepts and entrance boundary layer conditions. The blowing configurations include discrete tangential jets at various distributions, blowing vortex generators, vortex generators plus jets, and a variety of canted blowing holes. Each of these boundary layer control techniques could also have been modeled within a computational analysis in a similar manner as the vortex generator case previously discussed.

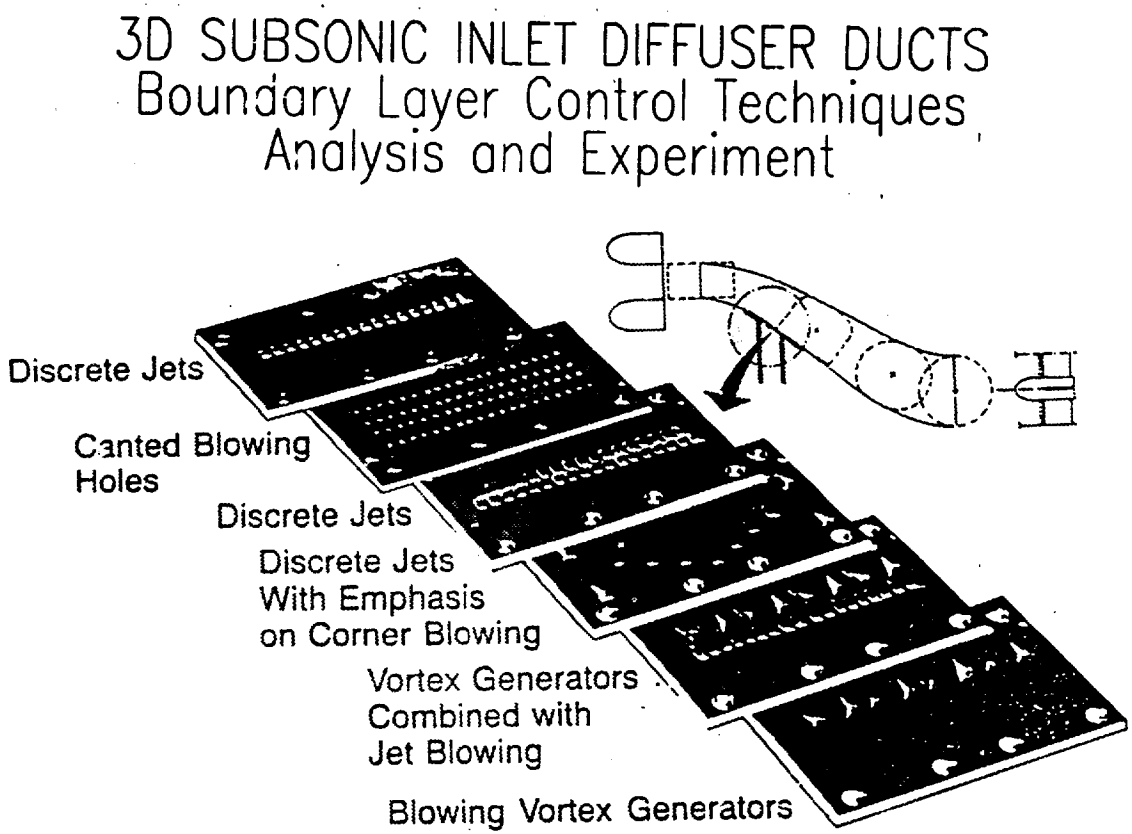

CFD FOR INLET AIRFRAME INTEGRATION
A Modern Viewpoint

"Even when available CFD tools are not extremely precise, they often have been used to aid the designers in what might be called a semiquantitative fashon. The importance of this concept follows the well known principle that if one can show an engineer where the flow goes and why (qualitatively) then he can usually figure out how to control it better"

Current Capabilities and Future Direction
in
Computational Fluid Dynamics

EFFECT OF VORTEX INGESTION ON THE INTERNAL FLOW FIELD OF 3D INLET DIFFUSER DUCTS

A series of calculation were performed on a family three inlet diffuser ducts at an enterence Mach Number of 0.5 and Reynolds number (based on enterence hydralic diameter) of 0.611x10e5 to investigate the effects of vortex ingestion on the internal flow field structure. Each of the three inlet diffuser ducts transitioned from an elliptical enterence (with the minor axis having a length ratio of 0.718 and major axis of 2.058) to a circular cross section of radius ratio 1.19 at the compressor face, in a dimensional length of 10.0. The area ratio (Aexit/Ainlet) was 1.42 for each of the configurations. The reference baseline duct (F30 configuration) had a streight centerline, while the F20 configuration had and inplane offset of 0.2 and the F10 configuration had an out-of-plane offset of 0.2.

The enterence flow field was established by centering a vortex having solid body rotation of prescribed swirl angle and allowing the governing equation to establish the initial starting conditions through an iteritative process where the solid body boundary conditions were held fixed. The swirl angle was varied from 0.0 degrees to 30.0 degrees, and included an initial boundary layer thickness of 0.2, relative to the local duct radius. It must be understood that the enterence conditions to a real duct in which vortex ingestion has taken place is unknown and must be determined experimentally, however this study seeks only to represent the starting conditions in a generic sense.

The movie sequence traces the vortex development through the F10 and F20 inlet ducts. including the interaction with a large separation that was present in both these ducts, with the purpose in mind to begin to study complex forebody-inlet interaction problems.

Effect of Vortex Ingestion on the Internal Flow Field of 3D Offset Inlet Diffuser Ducts

Straight Centerline Baseline Duct

Inplane Offset Diffuser Duct

Out-of-Plane Offset Diffuser Duct

F20 COMPUTATIONAL STUDY INLET
Geometry Definition, Downstream View
In-Plane Offset, Offset/Length = 0.2
Aexit/Ainlet = 1.42

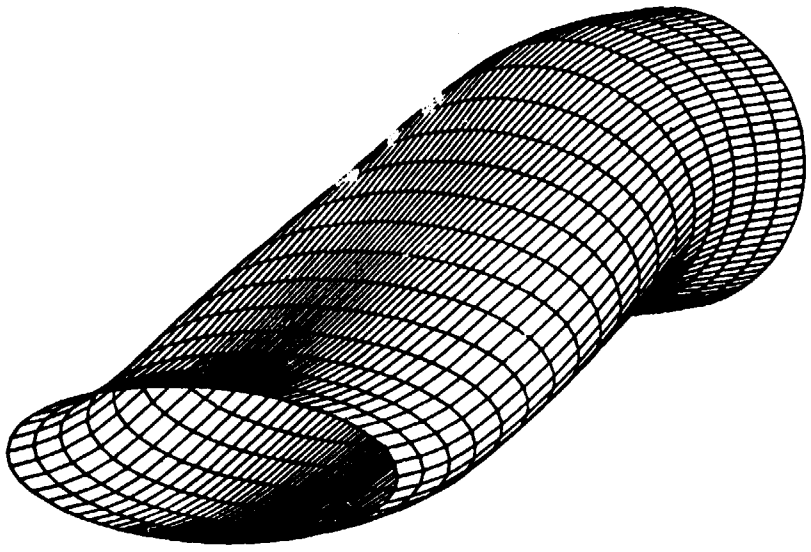

F30 COMPUTATIONAL STUDY INLET
Geometry Definition, Downstream View
Straight Centerline Inlet Duct
Aexit/Ainlet = 1.42

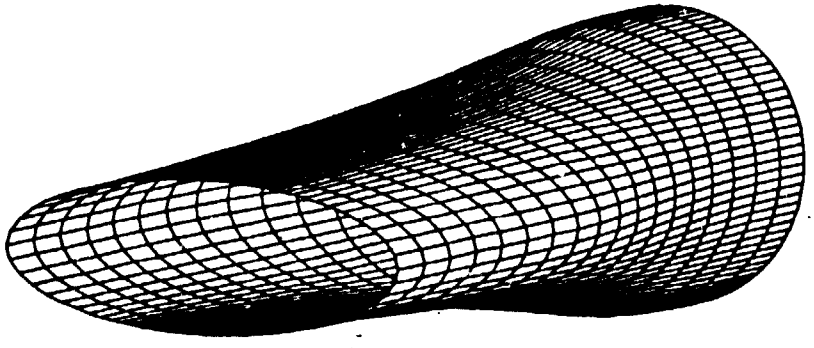

F10 COMPUTATIONAL STUDY INLET
Geometry Definition, Downstream View
Out-of-Plane Offset, Offset/Length = 0.2
Aexit/Ainlet = 1.42

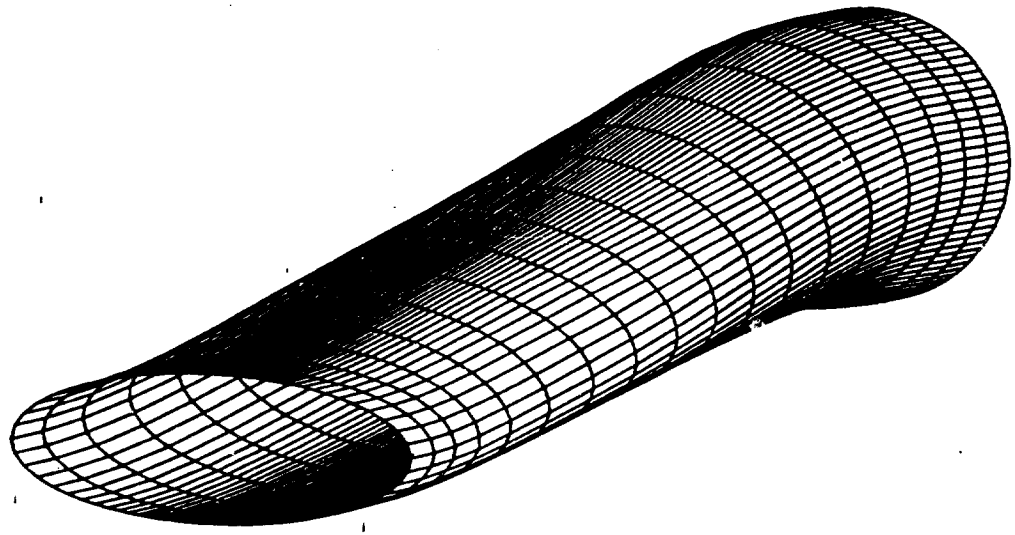

DESIGN OF A VALIDATION EXPERIMENT TO STUDY CONFINED SEPARATION IN CURVED DIFFUSING DUCTS

The philosphy underlying this section is that there needs to be an orderly progression in the development of the numerical modeling of complex turbulent flows, which go hand-in-hand with experiments designed to test the accuracy of numerical results, as well as provide fundamental understanding of the flow physics involved. The objective of this study is to provide a detailed experimental data base for the evaluation of Parabolized Navier Stokes (PNS) and Full Navier Stokes (FNS) codes to predict confined separation in curved diffusing ducts. The critical issue in this class of curved duct flows centers on the turbulence model, and its ability to describe accurately confined turbulent separation; that is, turbulent flow separation and reattachment confined within the duct. However, the PNS solver has the additional approximation of "flare type" modeling for regions of confined separation. Therefore defining regions where "flare type" approximations are applicable, in the sense that the global effect of the separation on the main flow is captured, can only be achieved by comparison with substantial 3D data sets for laminar flow separation. In addition, in order to conclusively establish that any FNS or PNS code can indeed capture the flow physics of confined separation, these codes must predict the change in the three dimensional separation topology as it is affected by Reynolds Number and initial conditions, which include both boundary layer thickness and swirl effects. Thus, the experimental test matrix must be designed to provide an accurate data base of sufficiently wide range for both laminar and turbulent separation to substantiate that the physics of flow separation and reattachment are captured.

Design of a Validation Experiment to Study Confined Separation in Curved Diffusing Ducts

CFD VALIDATION EXPERIMENT

Models	A Circular Arc ($R/r = 5.6$) Round Diffuser of Area Ratio 1.5 will be Arranged in the Form of two Connecting 90.0 Degree Bends so as to Allow a 180 degree Inplane, 90–90 out–of–plane, and 90–90 Inplane Diffusing Duct
Conditions	For Each Duct, Three Sets of Separated Flow Data will be Obtained; for Laminar Flow at Nominal Reynolds Number of 500 and 1093, and Turbulent Flow at a Reynolds Number of 43,000
Analysis	A Pre–Test Analysis will be Performed to Establish the Flow Separation Topologies and how they are Effected by Reynolds Number, Boundary Layer Thickness, and Swirl
Measurments	Experiments will be Carried out with Combinations of Laser–Velocimetry, Hot Wire Anenometry, Pressure Tubes, and Flow Visualization. Survey Planes will be Established from Analysis of the Computational Results

CFD VALIDATION EXPERIMENT

Title	Confined Separation in Curved Diffusing Ducts
Objective	Establish a Detailed Experimental Data Base for Evaluation of Navier Stokes Codes for Confined Separated Flows in Curved Diffusing Ducts
Thrusts	Extension and Validation of Lewis PNS Solver into Separated Flow Regime using Flare Approximations Evaluation and Extension of State–of–the–Art Tu–Models for Confined, Separated, Swirling Flows Evaluation and Validation of Lewis Time Marching NS Solver (PROTEUS) into Separated Flow Regime
Approach	A Joint Analysis/Experimental Program will be Initiated in which the Experimental Measurments will be Performed at a University, and the Analysis at Lewis Research Center

CONFINED SEPARATION IN CURVED DIFFUSING DUCTS
CFD Validation Cases

Reynolds No.	Flow	δ/R	Swirl Angle	Conf. 1	Conf. 2	Conf. 3
500.0	Laminar	0.2	0.0	CS	CS	CS
			30.0	CS	CS	CS
			45.0	CS	CS	CS
		1.0	0.0	CS	CS	SF
			45.0	CS	CS	CS
1093.0	Laminar	0.2	0.0	CS	CS	SF
			30.0	CS	CS	SF
			45.0	CS	CS	CS
		1.0	0.0	CS	SF	SF
			45.0	CS	SF	SF
43,000	Turbulent	0.2	0.0	CS	CS	SF
			15.0	CS	CS	CS
			30.0	CS	CS	CS
		1.0	0.0	CS	SF**	SF**
			30.0	CS	CS	CS

AF – Attached Flow CS – Confined Separation SF – Separated Flow

CFD VALIDATION DIFFUSING DUCTS
180 Degree Inplane Geometry
Configuration No. 1

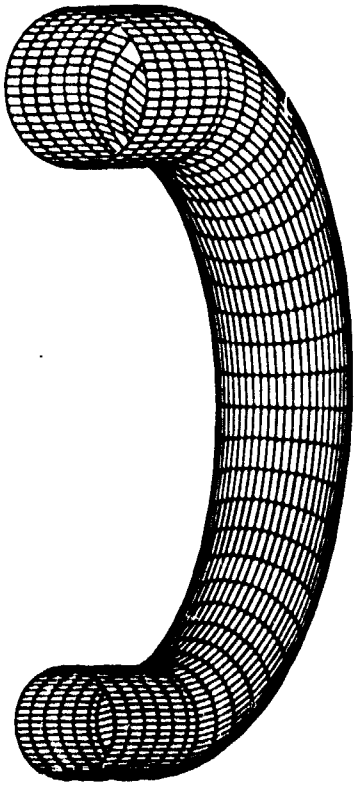

CFD VALIDATION DIFFUSING DUCTS
90/90 Out-of-Plane Geometry
Configuration No. 2

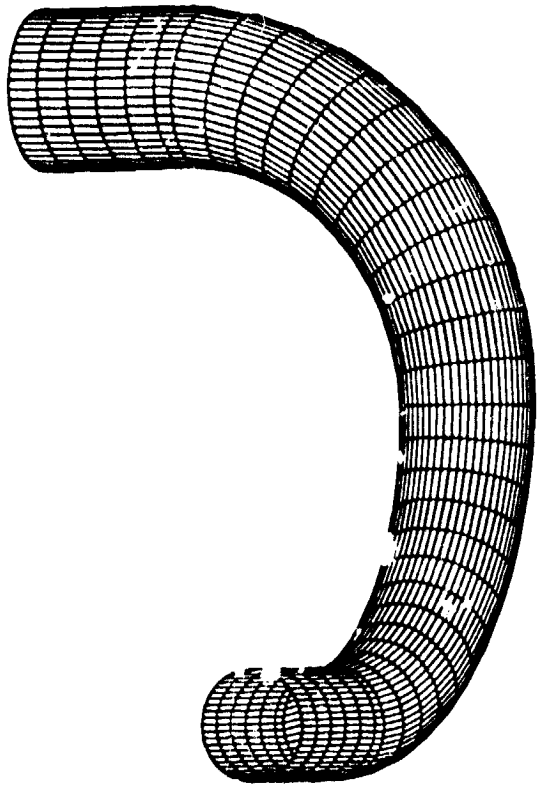

CFD VALIDATION DIFFUSING DUCTS
90/90 Degree Inplane Geometry
Configuration No. 3

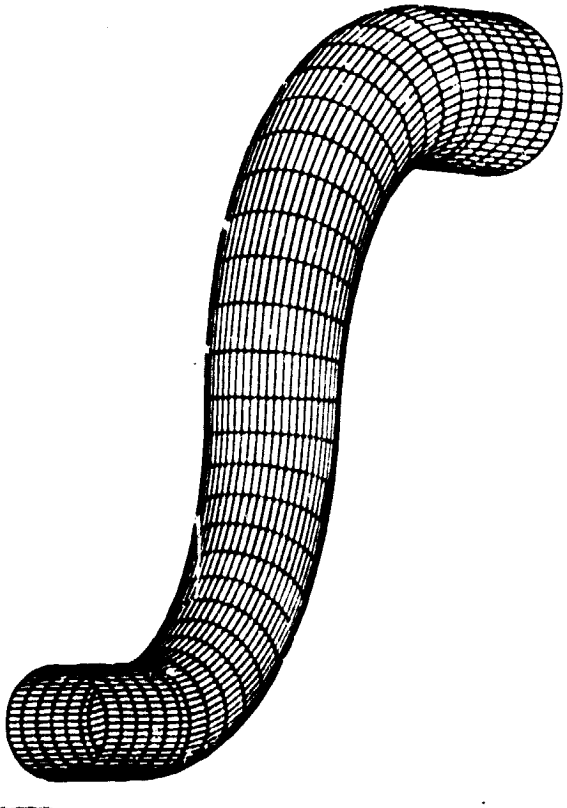

CFD FOR INLET AIRFRAME INTEGRATION

A Future Perspective

CFD for Inlet Airframe Integration has opened a new realm of capability for the design engineer in that, for the first time in history, the intricate features of complex flow can be computed. This new capability in turn has set the stage for new levels of understanding of the fluid flows, once the the researcher or designer is satisfied that the code's numerical algorithm and physical modeling accurately represent the critical physics of the flow. This confidence can only be gained by detailed comparison with experimental data of sufficient accuracy and detail to verify the CFD capability. These types of experiments are called "Benchmark" or "Validation" experimemts, and afford the researcher the opportunity to study and understand the highly complex three dimensional viscous flows from a building block concept. Thus CFD has introduced "Analysis Based Design" into the design system, where analysis and fundamental understanding replace trial-and-error and "Matrix Testing".

With close interaction between CFD and experimentation, advanced computer programs will be used both to design an experiment and to predict the results so that the the test, or design, is under control at all times, But this interaction also gives the researcher a fundamental understanding of the fluid processes that are important to the inlet airframe system. This is the main idea of this seminar series on a "User's Technology Guide to CFD Inlet Airframe Integration".

CFD FOR INLET AIRFRAME INTEGRATION
A Future Perspective

"With close interplay of CFD and experimentation, advanced computer programs will be used both to design an experiment and predict the results so that the test (or design) is under control at all times"

Current Capabilities and Future Direction
in
Computational Fluid Dynamics

REFERENCES AND BIBLIOGRAPHY

1. McDonald, H. and Briley, W. R., "Three-Dimensional Supersonic Flow of a Viscous or Inviscid Gas," J. Comp. Phys., Vol. 19, pp. 150-178, October 1975.

2. Buggeln, R. C., McDonald, H., Levy, R. and Kreskovsky, J. P., "Development of a Three Dimensional Supersonic Inlet Flow Analysis," NASA CR-3218, January 1980.

3. Buggeln, R. C., McDonald, H., Kreskovsky, J. P. and Levy, R., "Computation of Three Dimensional Supersonic Flow in Inlets," AIAA Paper No. 80-0194, January 1980.

4. Buggeln, R. C., McDonald, H. and Kim, Y. W., "Computation of Multi-Dimensional Viscous Supersonic Flow by Spatial Forward Marching," AIAA Paper No. 83-0177, January 1983.

5. Buggeln, R. C., McDonald, H., and Kim, Y. W., "Computation of Multi-Dimensional Viscous Flow by Spatial Forward Marching," (NASA CR in preparation).

6. Briley, W. R. and McDonald, H., "Solution of the Multidimensional Compressible Navier Stokes Equations by a Generalized Implicit Method," J. Comp. Phys., Vol. 24, p. 372, August 1977

7. Briley, W. R. and McDonald, H., "On the Structure and Use of Linearized Block Implicit Schemes," J. Comp. Phys., Vol. 34, January 1980.

8. McDonald, H. and Briley, W. R., "Computational Fluid Dynamic Aspects of Internal Flows," AIAA Paper No. 79-1445, July 1979.

9. McDonald, H., Shamroth, S., and Briley, W. R., "Transonic Flow with Viscous Effects," Transonic, Shock and Multidimensional Flows, Academic Press, 1982.

10. Douglas, J. and Gunn, J. E., "A General Formulation of Alternating Direction Methods Part I Parabolic and Hyperbolic Problems," Numerishe Math., Vol. 6, July 1964.

REFERENCES AND BIBLIOGRAPHY

11. Briley, W. R., "Numerical Method for Predicting Three-Dimensional Steady Viscous Flow in Ducts," J. Comp. Phys., Vol. 14, pp. 8-28, January 1974.

12. Eiseman, P. R., McDonald, H. and Briley, W. R., "A Method for Computing Three-Dimensional Viscous Diffuser Flows," UARL Report R75-911737, July 1975.

13. Roscoe, D. V., Shamroth, S. J., Gibeling, H. J., and McDonald, H., Investigation of the Mechanism of Transonic Shock Wave/Boundary Layer Interactions Using a Navier Stokes Analysis," SRA Rep. R83-930006-F, October 1983.

14. Liu, N. S., Shamroth, S. J., and McDonald, H., "Numerical Solution of the Navier-Stokes Equations for Compressible Turbulent Two/Three Dimensional Flows in the Terminal Shock Region of an Inlet/Diffuser," AIAA Paper No. 83-1892, July 1983.

15. Liu, N. S., Shamroth, S. J., and McDonald, H., "Numerical Solution of the Navier-Stokes Equations for Compressible Turbulent Two/Three Dimensional Flows in the Terminal Shock Region of an Inlet/Diffuser," NASA CR 3723, August 1983.

16. Liu, N. S., Shamroth, S. J., and McDonald, H., "Dynamic Response of Shock Waves in 2-D Transonic Diffuser and Supersonic Inlets." (Report in preparation).

17. Briley, W. R., Kreskovsky, J. P., and McDonald, H., "Computation of Three-Dimensional Viscous Flow in Straight and Curved Ducts," UTRC Report R76-911841, August 1976.

18. Eiseman, P. R., Levy, R., McDonald, H., and Briley, W. R., "Development of a Three Dimensional Turbulent Duct Flow Analysis," NASA CR 3029, November 1978.

19. Levy, R., McDonald, H., Briley, W. R., and Kreskovsky, J. P., "A Three-Dimensional Turbulent Compressible Subsonic Duct Flow Analysis for Use with Constructed Coordinate Systems," NASA CR 3389, April 1981.

20. Levy, R., Briley, W. R., and McDonald, H., "Viscous Primary/Secondary Flow Analysis for Use with Nonorthogonal Coordinate Systems," AIAA Paper No. 83-0556, January 1983.

REFERENCES AND BIBLIOGRAPHY

21. Briley, W. R., and McDonald, H., "Analysis and Computation of Viscous Subsonic Primary and Secondary Flows," AIAA Paper No. 79-1453, July 1979.

22. Fukuda, M. K., Hingst, W. R. and Reshotko, E., "Control of Shock-Wave Boundary Layer Interactions by Bleed in Supersonic Mixed Compression Inlets," NASA CR 2595, August 1975.

23. Anderson, W. E. and Wong, N. D., "Experimental Investigation of a Large Scale, Two-Dimensional, Mixed-Compression Inlet System - Performance at Design Conditions, M=3.0," NASA TM X-2016, May 1970.

24. Syberg, J., and Hickcox, T. E., "Design of a Bleed System for a Mach 3.5 Inlet," NASA CR 2187, January 1973.

25. Gnos, A. V. and Watson, E. C., "Investigation of Flow Fields within Large-Scale Hypersonic Inlet Models," NASA TN D-7150, April 1973.

26. Rose, W. C., "Behavior of a Compressible Turbulent Boundary Layer in a Shock Wave Induced Adverse Pressure Gradient," PhD Thesis, Univ. of Washington, 1972. Also NASA TN D-7092, March 1973.

27. Oskam, B., Vas, I. E. and Bogdonoff, S. M., "Mach 3.0 Oblique Shock Wave/Turbulent Boundary Layer Interaction in Three Dimensions," AIAA Journal, Vol. 16, No. 10, pp. 1090-1096, December 1976.

28. Oskam, B., Vas, I. E. and Bogdonoff, S., "Oblique Shock Wave/Turbulent Boundary Layer Interaction at Mach 3.0," AFFDL-TR-76-48, Part I, June 1976.

29. Oskam, B., Vas, I. E. and Bogdonoff, S., "Oblique Shock Wave/Turbulent Boundary Layer Interaction at Mach 3.0," AFFDL-TR-76-48, Part II, March 1978.

30. Rainbird, W. J., "Turbulent Boundary Layer Growth and Separation on a Yawed Cone," AIAA Journal, pp 2410-2416, December 1968.

REFERENCES AND BIBLIOGRAPHY

31. Hingst, W. R. and Tanji, F. T., "Experimental Investigation of a Two-Dimensional Shock-Turbulent Boundary Layer Interaction with Bleed," NASA TM 83057, (Also AIAA Paper No. 83-0135), January 1983.

32. Cresci, R. J., "Hypersonic Flow along Two Intersecting Planes," AFOSR Report 66-0500, March 1966.

33. West, J. E., and Korkegi, R. H., "Supersonic Interaction in the Corner of Intersecting Wedges at High Reynolds Numbers," AIAA Journal, Vol 10, No. 5, pp 652-656, May 1972.

34. Settles, G. S., Perkins, J. J., and Bogdonoff, S. M., "Upstream Influence Scaling of 2D & 3D Shock/Turbulent Boundary Layer Interactions at Compression Corners," AIAA Paper No. 81-0334, January 1981.

35. Anderson, B. H. and Towne, C. E., "Numerical Simulation of Supersonic Inlets Using a Three-Dimensional Viscous Flow Analysis," NASA TM 81411, (Also AIAA Paper No. 80-03840), January 1980.

36. Anderson, B. H., and Benson, T. J., "Numerical Solution to the Glancing Sidewall Oblique Shock Wave/Turbulent Boundary Layer Interaction in Three Dimensions," NASA TM 83056, (Also AIAA Paper No. 83-0136), January 1983.

37. Benson, T. J., and Anderson, B. H., "Validation of a Three-Dimensional Viscous Analysis of Axisymmetric Supersonic Inlet Flow Fields," NASA TM 85038, (Also AIAA Paper No. 83-0135), January 1983.

38. Mateer, G. G., and Viegas, J. R., "Effect of Mach and Reynolds Number on a Normal Shock-Wave/Turbulent Boundary Layer Interaction," AIAA Paper No. 79-1502, July 1979.

39. Bogar, T. J., Sajben, M., and Kroutil, J. C., "Characteristic Frequency and Length Scale in Transonic Diffuser Flow Oscillation," AIAA Paper No. 81-1291, 1981.

40. Salmon, T. J., Bogar, T. J., and Sajben, M., "Laser Velocimeter Measurements in Unsteady, Separated, Transonic Diffuser Flows," AIAA Paper No. 81-1197, 1981.

REFERENCES AND BIBLIOGRAPHY

41. Sajben, M., Bogar, T. J., and Kroutil, J. C., "Forced Oscillation Experiments in Supercritical Diffuser Flows with Application to Ramjet Instabilities," AIAA Paper No. 81-1487, 1981.

42. Briley, W. R., Buggeln, R. C., and McDonald, H., "Computation of Laminar and Turbulent Flow in 90 Degree Square Duct and Pipe Bends Using the Navier-Stokes Equations," SRA Rpt. R82-920009, 1982.

43. Rowe, M., "Measurements and Computations of Flow in Pipes," J. Fluid Mech., Vol. 43, p. 771-783, 1970.

44. Taylor, A. M. K. P., Whitelaw, J. H. and Yianneskis, M., "Measurement of Laminar and Turbulent Flow in a Curved Duct with Thin Inlet Boundary Layers," NASA CR 3367, January 1981.

45. Enayet, M. M., Gibson, M. M., Taylor, A. M. K. P., and Yianneskis, M., "Laser Doppler Measurements of Laminar and Turbulent Flow in a Pipe Bend," NASA CR 3551, May 1982.

46. Agrawal, Y., Talbot, L and Gong, K., "Laser Anemometer Study of Flow Development in Curved Circular Pipes," J. Fluid Mechanics, Vol. 85, pp 497-516, 1978.

47. Taylor, A. M. K. P., Whitelaw, J. H., and Yianneskis, M., "Developing Flow in S-Shaped Ducts, Part I-Square Cross Section Ducts," NASA CR 3550, May 1982.

48. Taylor, A. M. K. P., Whitelaw, J. H., and Yianneskis, M., "Developing Flow in S Shaped Ducts Part II: Circular Cross-Section Duct," (NASA CR in preparation).

49. Bansod, P., and Bradshaw, P., "The Flow in S-Shaped Ducts," Aeronautical Quarterly, vol. 23, pp 131-140, May 1972.

50. Taylor, A. M. K. P., Whitelaw, J. H., and Yianneskis, M., "Turbulent Flow in a Square-to Round Transition," NASA CR 3447, July 1981.

REFERENCES AND BIBLIOGRAPHY

51. Vakili, A., Wu, J. M., Hingst, W. R., and Towne, C. E., "Comparison of Experimental and Computational Compressible Flow in an S-Duct," AIAA Paper No. 84-003, January 1984.

52. Towne, C. E., and Anderson, B. H., "Numerical Simulation of Flows in Curved Diffusers with Cross-Sectional Transitioning Using a Three-Dimensional Viscous Analysis," NASA TM 81672, (Also AIAA Paper No. 81-0003), January 1981.

53. Towne, C. E., "Computations of Viscous Flow in Curved Ducts and Comparison with Experimental Data," AIAA Paper No. 84-0531, January 1984.

54. Anderson, B. H., Putt, C. W., and Giamati, C. C., "Application of Computer Generated Color Graphic Techniques to the Processing and Display of Three Dimensional Fluid Dynamic Data," NASA TM 82658, November 1981.

55. Anderson, B. H., Putt, C. W., and Giamati, C. C., "Fluid Dynamic Data-In Color and Three Dimensions," Mechanical Engineering, pp. 30-35, March 1982.

56. Vakili, A. D., Wu, J. M., Liver, P., and Bhat, M. K., "Experimental Investigation of Secondary Flow in a Diffusing S-Duct," (Warren Hingst Project Manager, NASA Lewis Research Center, to be published), 1986

57. Campbell, A.F., and Forester, C.K., "Evaluation of a Method for Analyzing the Aperture Region of Two-Dimensional External Compression Inlets", AIAA Paper No. 85-3072, October 1985.

58. Howlett, D.G. and Hunter, L.G., "A Study of a Supersonic Axisymmetric Spiked Inlet at Angle of Attack Using the 3-D Navier Stokes Equations", AIAA Paper No. 86-0308, January 1986.

59. Newsome, R.W.,"Numerical Simulation of Near-Critical and Unsteady Subcritical Inlet Flow Fields," AIAA Paper No. 83-0175, January 1983.

60. Kumar, Ajay, "Numerical Analysis of a Scramjet Inlet Flow Field Using the Three-Dimensional Navier-Stokes Equations," JANNAF Propulsion Meeting, February 1983.

REFERENCES AND BIBLIOGRAPHY

61. Kunik, W.G., Benson, T.J., Ng, W-F, and Taylor, A., "Two- and Three-Dimensional Viscous Computations of a Hypersonic Inlet Flow," AIAA Paper No. 87-0283, January 1987.

62. Bushnell, D.M., and Beckwith, I.E., "Calculation of Nonequilibrium Hypersonic Turbulent Boundary Layers and Comparisons with Experimentl Data," AIAA Journal Vol. 8, No. 8, pp 1462-1469,

63. Current Capabilities and Future Direction in Computational Fluid Dynamics," National Acadamy Press, Washington, D.C., 1986

64. Anderson, B. H.: "Three Dimensional Viscous Design Methodology of Supersonic Inlet Systems for Advanced Technology Aircraft", AIAA 84-0194, 1984. August 1970.